Journal of Materials Chemistry A

REVIEW

View Article Online
View Journal | View Issue

Check for updates

Cite this: J. Mater. Chem. A, 2023, 11, 10473

Prussian blue and its analogues as functional template materials: control of derived structure compositions and morphologies

Behnoosh Bornamehr, [ab] Volker Presser, *[abc] Aldo J. G. Zarbin, *[d] Yusuke Yamauchi *[ef] and Samantha Husmann *[a]

Received 6th December 2022
Accepted 17th February 2023

DOI: 10.1039/d2ta09501g

rsc.li/materials-a

Hexacyanometallates, known as Prussian blue (PB) and its analogues (PBAs), are a class of coordination compounds with a regular and porous open structure. The PBAs are formed by the self-assembly of metallic species and cyanide groups. A uniform distribution of each element makes the PBAs robust templates to prepare hollow and highly porous (hetero)nanostructures of metal oxides, sulfides, carbides, nitrides, phosphides, and (N-doped) carbon, among other compositions. In this review, we examine methods to derive materials from PBAs focusing on the correlation between synthesis steps and derivative morphologies and composition. Insights into catalytic and electrochemical properties resulting from different derivatization strategies are also presented. We discuss challenges in manipulating the derivatives' properties, give perspectives of synthetic approaches for the target applications and present an outlook on less investigated grounds in Prussian blue derivatives.

Open Access Article. Published on 15 March 2023. Downloaded on 2/9/2026 11:49:42 AM.
This article is licensed under a Creative Commons Attribution 3.0 Unported Licence.

1. Introduction

Prussian blue (PB) is a well-known classic coordination compound that has risen from an old painting pigment to a widely studied electrode material.[1] PB and its analogues (PBAs) combine the presence of redox-active metallic species and an open porous structure that can accommodate ions with little or no volumetric change. Such characteristics are attractive for energy storage, catalysis, sensing, and biomedical applications, among others.[2–5] Recently, PBAs have gained growing interest as a template material for preparing porous derivatives.[6,7] By providing metal species, carbon, and nitrogen from cyanide ligands combined with a well-structured, stable, and highly porous framework, they enable sacrificial templating (or template-engaged/self-template) methods. Templating is a very effective tool to synthesize more complex porous and hollow structures, and many different (hetero)nanostructures derived from PBAs have already been described.[8–10] Calcination methods produce oxides,[11–13] while annealing generates carbides,[14,15] alloys,[16,17] or metal nanoparticles with different compositions.[18–22] Pre-treatments can regulate the morphology of the derivatives or introduce heteroatoms.[22–24]

Nevertheless, fast and simultaneous reports within the past few years have led to many PBA derivative (hereafter referred to as PBDs) compositions and morphologies with little control over the product, where even different derivatives are obtained under similar processing conditions. This lack of understanding of how PBA characteristics and the derivatization process affect the composition, structure, and morphology of PBDs, makes the control and prediction of the final product a current challenge. Despite that, PBDs perform very well in electrocatalysis, batteries, and capacitors, far surpassing counterparts obtained by different methods. A comprehensive summary of the PBA derivatization methods and correlation with PBD composition, morphology, and properties is particularly interesting in this context.

Most reviews on PBDs focus on specific applications such as energy storage,[6,9,10,25] catalysis,[10,26] and the environment.[9] Nevertheless, very few describe the synthetic methods to obtain PBDs; noteworthy are the compilation of Fe-based PBDs prepared by Li *et al.*,[13] and the revisions of Zakaria *et al.*[27] and Azhar *et al.*[28] that largely focus on PBA modification prior to derivatization. The growing chemical compositions and structure complexity described for PBDs require an overview of the synthesis routes and steps and the approaches utilized for each composition group (oxides, sulfides, carbides, *etc.*).

[a]INM – Leibniz Institute for New Materials, Campus D2 2, 66123, Saarbrücken, Germany. E-mail: volker.presser@leibniz-inm.de; husmann.samantha@gmail.com
[b]Department of Materials Science & Engineering, Saarland University, Campus D2 2, 66123, Saarbrücken, Germany
[c]Saarene – Saarland Center for Energy Materials and Sustainability, Campus C4 2, 66123 Saarbrücken, Germany
[d]Department of Chemistry, Federal University of Paraná (UFPR), CP 19032, 81531-980 Curitiba, PR, Brazil. E-mail: aldozarbin@ufpr.br
[e]School of Chemical Engineering and Australian Institute for Bioengineering and Nanotechnology (AIBN), The University of Queensland, Brisbane, QLD 4072, Australia. E-mail: y.yamauchi@uq.edu.au
[f]International Center for Materials Nanoarchitectonics (WPI-MANA), National Institute for Materials Science (NIMS), 1-1 Namiki, Tsukuba, Ibaraki 305-0044, Japan

Open Access Article. Published on 15 March 2023. Downloaded on 2/9/2026 11:49:42 AM. This article is licensed under a Creative Commons Attribution 3.0 Unported Licence.

In this review, we introduce the concept of using the PB family of compounds as template materials and present their characteristics and advantages, and their potential to be used as precursors for novel materials. In addition, we will examine the strategies adopted in the PBA synthesis to create specific template structures. The different derivatization methods will be summarized in terms of composition and morphology, addressing the approaches for introducing additional elements and creating complex structures. This will provide a guide map for the derivatization of new compositions and gives a better insight into planning the synthesis route for the intended application. As many of the derivatives are used as catalysts and energy storage electrodes, some examples of different processing methods for PBD fabrication and the effect of the steps and the attained morphology on the performance in these specific applications will be demonstrated. Finally, we will elaborate on the key aspects of PBA templating that dictate the composition and morphology of the derivatives and will discuss the challenges in achieving control over material design.

2. Prussian blue and its analogues as template materials

Prussian blue is the oldest reported coordination compound, yet it is still the subject of intense research to the present day.[9] PB was initially discovered as a pigment at the beginning of the 18th century. However, after its structural characterization and discovery of its redox properties in the 1970s,[29,30] this material found interest in other areas of application such as (bio)sensors and absorption, filtration and purification, energy storage and conversion, and drug delivery, among others.[31–33]

As coordination compounds, the primary structure of the PBA family is based on two metal centres bridged through cyanide ligands in an octahedral arrangement, formally denoted as hexacyanometallates. A PBA presents a general formula $A_xM[M'(CN)_6]_y\square_{1-y}\cdot nH_2O$, where M and M′ are transition metals coordinated to the nitrogen and carbon of CN ligands, respectively (Fig. 1A); A is normally an alkali cation, □ stands

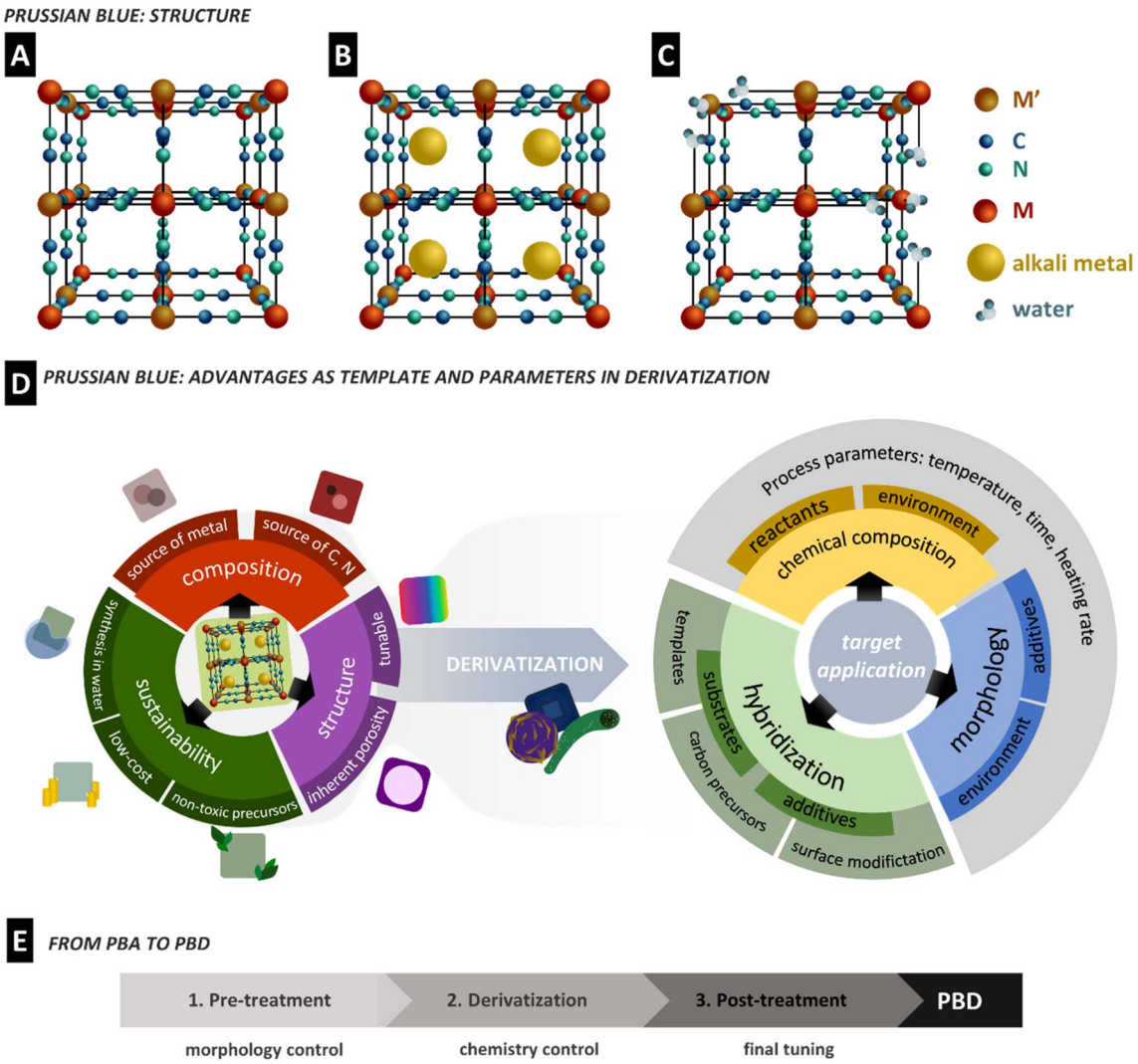

Fig. 1 (A) Theoretical PBA lattice. (B) Defect-free "soluble" PBA with alkali ions in the lattice. (C) "Insoluble" PBA lattice with defects and water molecules filling the defect sites. (D) PBA characteristics useful for templating and the parameters affecting the PBD properties. (E) The proposed approach for PBD derivatization in three steps, and the main feature of each step.

 This journal is © The Royal Society of Chemistry 2023

Open Access Article. Published on 15 March 2023. Downloaded on 2/9/2026 11:49:42 AM. This article is licensed under a Creative Commons Attribution 3.0 Unported Licence.

for possible lattice vacancies, and coordinated water can eventually occupy defects or uncoordinated sites. In the case of PB, the metal centres are Fe(III) and Fe(II) species, resulting in the formula $AFe^{III}[Fe^{II}(CN)_6]$. The defective and alkali-free structure is often referred to as insoluble, while the highly organized and alkali-containing one is defined as soluble PB (Fig. 1A–C).[10] These terms do not correlate with PBA solubility in water or solvents. The cubic structure formed from the octahedral coordination of both metals leads to a porous framework, while the strong bonding energy of the cyanide ligands gives rigidity to the material.[34] During redox reactions of the metallic centres, ions can be stored in the porous lattice, while the structure rigidity prevents significant strain or expansion, enabling stable ion insertion processes.[35] The properties and the size of the interstitial sites can be tuned by the metal character through replacing one or both Fe centres with several other transition metals such as cobalt, manganese, and nickel, leading to PBAs.[36] These characteristics combined allow a PBA to be selective towards specific ions, which has significant implications on its application performance and possibilities.[37,38]

In 1984, Itaya *et al.* demonstrated the catalytic effect of Prussian white (PB reduced form) on H_2O_2 reduction, which led to almost 40 years of exponential research on PB in analytical bio-sensors.[39] As a consequence, novel PBAs were described, bringing new electrochemical properties that naturally diversify PBAs' application as electrode materials. Much of PBAs outstanding performances arise from combining (multi) metallic centres and the described open framework structure, often compared to metal–organic frameworks (MOFs). Unlike MOFs, PBAs are water and air-stable under standard ambient conditions,[40] are easy to synthesize, and present a high concentration of redox-active species per cell volume. In addition, the short cyanide ligands create easy access to the metallic species while holding the structure, which is often a drawback of the bulky ligands in MOFs.[41,42] Though restricted in terms of ligand nature, PBAs with many different combinations of transition metals have been described.[11]

An appealing characteristic of PBAs to be used as a template is that they are biocompatible.[43] At the same time, their synthesis is normally performed by a fast, easy, and water-based co-precipitation method using relatively cheap precursors. It is cost-effective and shows a high degree of sustainability. The co-precipitation synthesis of PBAs generally consists of the dropwise addition of an MX salt solution ($X = Cl^-$, NO_3^-, SO_4^{2-}, *etc.*) to a solution of $A_{6-x}[M'^{x}(CN)_6]$. The M ion coordinates to the $[M'^{x}(CN)_6]$ unit, while A ions can be incorporated into the structure in a generic reaction that can be expressed as:

$$M^{y+}_{(aq)} + [M'^{x+}(CN)_6]^{(6-x)-}_{(aq)} + (6 - x - y)A^+ \rightarrow (A_{(6-x-y)}M[M'(CN)_6]_y \cdot nH_2O)_s$$

Parameters like the concentration of precursors, pH, temperature, and mixing rate, among others, influence the composition, crystallinity, defect content, and particle size.[44,45] Surfactants or carbonaceous materials are often added to control the shape or reduce the particle size. In contrast, additional M salts can be added during co-precipitation to produce more complex compositions,[15,28] resulting in a gradient composition between two (or more) PBAs.[46,47] An intrinsic parameter that affects the particle size is the solubility of the PBA and therefore, its formation speed. This must be considered while changing the chemistry of the PBA and designing its size and morphology. The solubility difference can itself be used to stabilize unstable PBAs. For example, a core–shell PBA on PBA structure can be synthesized by covering soluble vanadium hexacyanoferrate (VHCFe) with copper hexacyanoferrate (CuHCFe), which has a lower solubility.[48] The synthetic approaches and the interplay of the controlling variables over PBA characteristics and morphology are extensively reviewed. These will not, therefore, be discussed in depth here.[28,49,50] Nevertheless, understanding PBA synthesis and particle growth is of great importance, as well as understanding their versatility in composition and morphology, as they influence the PBDs derived from such materials. Therefore, we recommend that anyone interested in the PBD topic investigate PBA synthesis literature to be able to successfully tailor PBDs.

PBA characteristics are often pursued in electrode materials, such as metal oxides and sulfides. Nano and microporosity are well known to benefit the electrochemical properties of materials as they increase the surface area, facilitate ion transport and improve electron mobility. Complex synthetic methods are often developed to achieve highly porous/hollow morphologies of well-known electrode materials and to improve performance.[51,52] In this context, PBAs have recently started to be used as templates to produce porous derivatives (Fig. 1D). Since the PBA structure benefits from the presence of C, N, and metallic elements, it can also accomplish self-templating.

Derivatization of PB and PBAs can be performed *via* multiple approaches, but thermal treatment is mostly used due to its versatility. By controlling the temperature and atmosphere, for example, using a carrier gas that reacts with the PBA, the derivative chemistry can be altered in various ways. Therefore, carbides, metal-containing compounds, or simply metal alloys can be derived through thermal treatment. Other methods, such as liquid and hydrothermal syntheses, have also been used to derive metallic compounds and show the diversity in the synthesis of PBDs, however, with far less extent compared to the thermal procedures.[27] The next section will provide an overview of the PBA derivatization strategies and steps through which different morphologies and compositions can be obtained.

3. PBD synthesis strategies

Synthesis of PBDs can be very versatile and sometimes lengthy; however, they can be roughly broken down into three main steps: pre-treatment, derivatization, and post-treatment. The derivatization is the key step, and it is defined here as the step that causes the conversion of a PBA into other materials (oxides, sulfides, carbides, *etc.*). Often a pre-treatment is performed before derivatization, occasionally followed by post-treatment to complete the entire procedure. Each of these steps is chosen strategically to result in a specific attribute of the

Open Access Article. Published on 15 March 2023. Downloaded on 2/9/2026 11:49:42 AM. This article is licensed under a Creative Commons Attribution 3.0 Unported Licence.

Table 1 Process steps and methods to achieve PBDs and their key features and limitations

Step	Method	Features	Limitations
Pre-treatment; modification of PBA characteristics	Template	Control of the macrostructure "Cubic-free" morphology possible Addition of new components/more complex composition Hollowness possible	Multi-step/time demanding Possible unwanted elements from the template
	Directed growth	Control of the microstructure (normally by using salt/surfactants) Normally achieved in one step High parameter sensibility: fine-tuning Hollowness and porosity possible (also combined with etching)	Less morphology variety than templates (cubic-derived morphology only) High parameter sensibility: difficult to control
	Etching	Added porosity and/or hollowness Time-dependent morphology: fine-tuning Combined with directed growth for morphological control	High sensibility to media and PBA characteristics Etching process depends on PBA crystallinity Particles >100 nm to avoid structure collapse Normally requires a combined hydrothermal process
	Ion exchange	Preparation of non-stable PBAs More complex M/M′ compositions Additional metals can be incorporated Combined with etching for control of exchanged ions and/or added porosity	Limited to specific ions (normally oxide/hydroxide salts) Not all metal species can be exchanged Generally limited to N-coordinated metal
	Coating	Control of the particle size Incorporation of additional elements that can be used in the derivatization step Protection against coarsening in derivatization	Normally limited to carbon coatings Sometimes, multi-step process/time demanding
	Hybrid/composite	Added functionality to PBAs and PBDs Added components can direct PBA growth but are not further removed	Not always homogeneous component distribution Possible reaction of an added component in the derivation process
Derivatization; conversion from a PBA to a PBD	Thermal	Accomplishes the widest variety of chemical compositions Time- and temperature-dependent compositions: tuning possible Possible porosity due to PBA shrinkage	Possible loss of morphology, especially at high T (coated samples can help mitigate) Less control over product than liquid-driven methods Sublimation or salt decomposition required for added elements (F, P, Se, *etc.*)
	Hydrothermal	Control of porosity through reaction time Larger variety of precursor salts Less energy intensive Can be combined with an acid/base for added porosity and hollowness Can produce an M′-free PBD with the aid of S-containing salts	Less variety in compositions compared to thermal Generally longer than thermal Normally requires a subsequent thermal step to add crystallinity
	Liquid	High complexity in morphology and metallic composition Can replace an N-coordinated metal	So far, limited to hydroxides So far, limited to pristine cubic PBAs Slower process
Post-treatment; final tuning of composition and morphology	Etching	Carbon products through metal leaching Addition of porosity and/or hollowness Removal of specific metallic species	Can cause morphology collapse Not all metals can be easily or selectively removed
	Thermal	Improved crystallinity Achieved carbon graphitization	Can cause morphology collapse Can modify composition during crystallization
	Composite	Added functionality to PBDs Versatility in composition and morphology Can support PB as a substrate	Lower interaction between the added component and PBD compared to pre-treatment Additional steps/time demanding

material, such as the morphological, physical, or chemical properties, and aid the material's performance in its target application. Each step can be taken *via* a single or multiple processes. For example, two pre-treatment strategies or two steps of derivatizations can be used. However, adding each step brings an extra challenge while extending time and energy

 This journal is © The Royal Society of Chemistry 2023

Open Access Article. Published on 15 March 2023. Downloaded on 2/9/2026 11:49:42 AM.
This article is licensed under a Creative Commons Attribution 3.0 Unported Licence.

demands. Pre-treatment steps are usually employed to control the morphology of the PBA, but morphology engineering is realizable only on particles with a minimum size to tolerate intricate architecture. Derivatization is the main step in defining PBD chemistry. However, this change in chemistry needs a high degree of control on process parameters to preserve the structure designed by pre-treatment. At last, post-treatment steps are used to fine-tune the product by etching away unwanted products or adding porosities, but this comes at the cost of high temperatures or the use of harsh acids. Therefore, understanding the full journey from a PBA to a PBD is essential to design an effective derivatization. A summary of the derivatization steps and methods covered in this review and an overview of their key features are described in Table 1.

3.1 Pre-treatment

Any treatment procedure that retains the PBA character, that is, being a hexacyanometallate, is considered a pre-treatment. Here, we summarize the strategies used in the pre-treatment to alter the PBA morphology and composition and make it ready for derivatization. These can be divided into templating and directed growth, etching, ion exchange, coating, and composite formation (Fig. 2A). We provide examples of the synthesis of PBA particles that were further used to prepare PBDs. The work on composition, morphology, and size control of PBA particles is extensive. Many pioneering and outstanding examples were left out simply because there is no work on producing PBDs from those structures, in particular, the anisotropic growth of PBAs to produce sheets, tubes, rods, or other nanostructures.[53,54] Most of the reported studies and the examples presented here are PBDs with cubic-derived morphology. This is evidence that many possibilities in PBD research remain unexplored.

3.1.1 Templating and directed growth. PBAs are sometimes synthesized through the templating strategy to control the particle shape and size. The templated PBA is then used as a template to form the PBD. Most PBAs naturally grow as cubic particles ranging from a few nanometers to a few micrometres, depending on the synthesis parameters such as solution concentration and temperature. The PBA templating strategies can act in two directions: introduce porosity and hollowness in the particle microstructure, or direct the macrostructure of the bulk material. PBAs can grow around the template material that is afterward removed to create hollow structures. This can be done, for example, through soft-templating by the use of polymers and surfactants, which are further removed, leaving a hollow PBA shell. By using different surfactants in $Co(NO_3)_2$ solution, Liu *et al.* were able to prepare different morphologies of cobalt hexacyanoferrate (CoHCFe).[55] The nature of the surfactant can direct how the particles will grow. In this example, sodium dodecyl benzene sulfonate (SDBS) forms droplets covered by the cobalt salt, leading to CoHCFe-covered SDBS spheres (Fig. 2B and C). Sodium dodecyl sulfate (SDS) covers the particle surface, producing SDS-covered CoHCFe cubes. Upon heat treatment of the PBA to produce FeCo oxides, the surfactant is removed, leading to porous cubes, hollow spheres, or nanoparticles.[55]

Hard templating has also been used to regulate the microstructure. Hard templating has the advantage of more flexibility in terms of shape and size due to the rigid structure compared to soft templates. Traditional methods like coating silicon particles and subsequent etching with acid can be employed for this. Nevertheless, a better way to induce hollowness and porosity is by using sacrificial templates, where the particle also takes part in the PBA reaction and is consumed, leaving an empty core. For example, Nai *et al.* prepared CoHCFe nanoframes in the presence of trisodium citrate.[56] Initially, typical cubes of CoHCFe are formed. However, with increased reaction time, the inner part of the cubes is consumed and reprecipitated at the edges of the original cubes, producing porous frames after 36 h of reaction. The citrate plays a key role as it protects the (100) faces of the cubes, leaving exposed reactive (110) edges. The size of the precursor cubes and the size of the resulting frames could also be tuned by using the concentration of the reactants. They observed that the soluble K-rich phase is the preferred structure at the frames compared to the inner cube, resulting in a less defective material.

Preferential growth engineering is a common approach in pre-treatment, and tailored morphologies can be synthesized based on the coverage of certain edges or faces of the crystal. For example, Nai *et al.*[57] explored epitaxial growth in CoHCFe to result in intricate structures such as frames, cages, and boxes. In this study, the initial PBA is formed rapidly, but over a longer holding time, a K-rich CoFe PBA starts forming on top of the original CoHCFe cubes. Due to higher activity at the corners and edges, the second phase starts nucleating from these sites. A higher growth rate was observed in the presence of PVP, and full coverage of the PBA template forms cages. Different citrate concentrations at this stage further ripened the shell into a solid or open frame. The authors explain the different morphologies by the different planes that PVP ([100]) and citrate ([111]) protect, and the influence of concentrations on the growth kinetics (Fig. 2D–F).[57]

Hard templating is a common approach for tuning the macrostructure of the particles. The template can function as a substrate for the growth of the PBA material, for example, using layered structures like graphene or MXenes to create PBA sheets, or wires to create PBA core–shell fibres or hollow tubes. Wang *et al.* used a nickel foam to grow different metallic structures like Co_3O_4 nanosheets, $Cu(OH)_2$ nanowires, or $Ni(OH)_2$ nanoparticles.[58] These materials were used as metal precursors to form different PBAs at the surface of the macrostructure. In this case, the template is not removed and takes part in the derivatization process, resulting in highly porous 3D structures.[58] This is a common strategy to guarantee that the template actively acts as a structure support, source of elements, or results in conductive carbon species.

3.1.2 Etching. Etching of a PBA is normally performed to achieve porosity and hollowness because this characteristic is desired in many applications for its high specific surface area. In the etching process, the etchant acts on the most reactive or weakest part, normally the corners or edges, producing cages.

Open Access Article. Published on 15 March 2023. Downloaded on 2/9/2026 11:49:42 AM.
This article is licensed under a Creative Commons Attribution 3.0 Unported Licence.

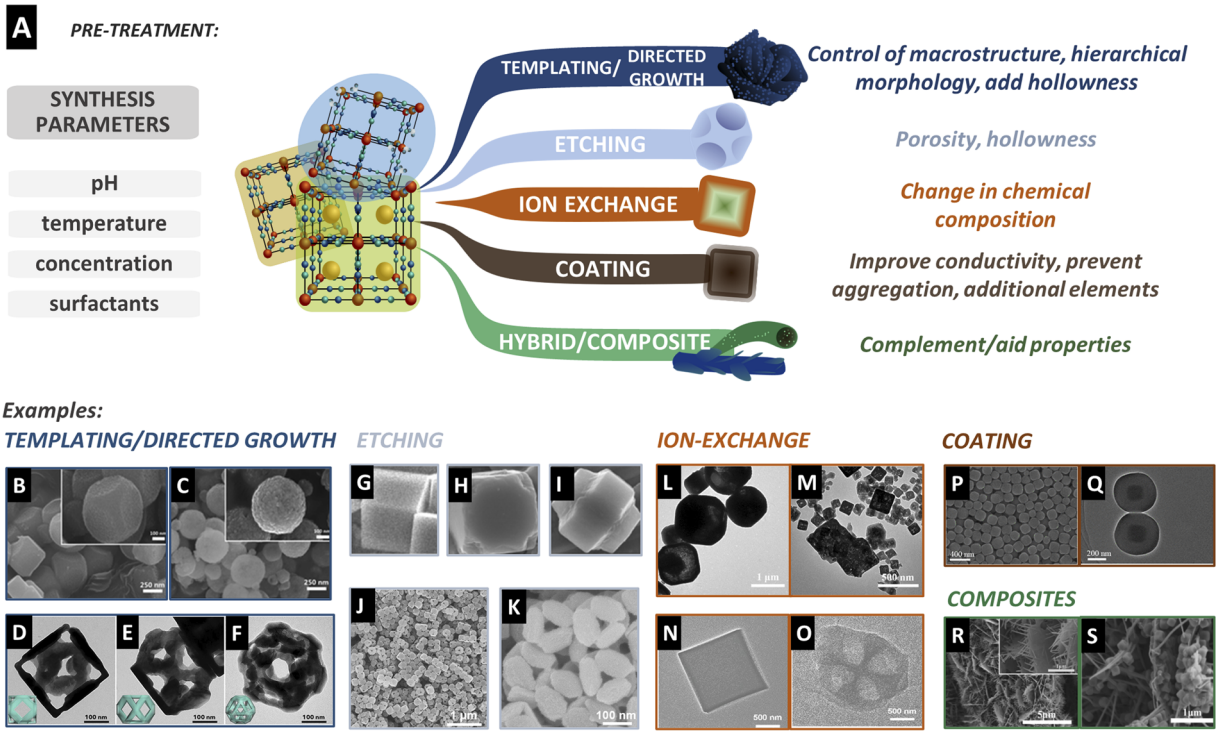

Fig. 2 (A) Strategies to modify PBA particles before derivatization, with the common target results. These treatments are performed in parallel to the synthesis parameters such as the pH, temperature, or concentration of the salts. (B) Co–Fe PBA precursor and (C) resulting porous spheres prepared by soft-templating. Reproduced from ref. [55] with permission from the Royal Society of Chemistry. (D–F) Directed growth of the CoHCFe precursor after resting in the presence of trisodium citrate. Reproduced with permission from ref. [57]. Copyright 2018 Elsevier. (G–I) Etching procedure of the cubic precursor in the presence of HCl[59] and (J and K) in the presence of ammonia.[23] (G–I) were reproduced from ref. [59] with permission from the Royal Society of Chemistry. (J and K) Were reproduced with permission from ref. [23]. Copyright 2017 WILEY-VCH Verlag GmbH & Co. KGaA, Weinheim. (L and M) TEM images of MnHCFe after the reaction with $Co(NO_3)_2$ in the absence (L) and presence (M) of C_2H_5OH creating porous CoHCFe cubes. Reproduced with permission from ref. [62]. Copyright 2021 Elsevier B.V. (N) Cubic precursors before and (O) after cation exchange due to the solubility difference. Reproduced with permission from ref. [22]. Copyright 2021 Wiley-VCH GmbH. (P) SEM image of the PB precursor and (Q) TEM image of core–shell spheres after coating with resorcinol formaldehyde. Reproduced with permission from ref. [67]. Copyright 2019 American Chemical Society. (R) NiCo arrays on carbon cloth as a substrate before and (S) after PBA cube formation. Reproduced with permission from ref. [75]. Copyright 2019 Elsevier B.V.

However, protective agents like polymers or surfactants can direct the etching process, for example, toward the cube faces, producing frames, or the interior, leading to hollow cubes. One of the first studies on the selective etching of PBAs was performed by Hu *et al.*, where the faces of PB cubes were protected by cetyltrimethylammonium bromide (CTAB), creating elongated cuboids in the presence of HCl.[59] In the absence of CTAB, the etching is random, while with its presence, a selectivity is observed for directional etching. In Fig. 2G–I, the etching of the cubes from corners, which have higher energy, is shown overtime, leading to the elongated-cube morphology, while faces are protected by CTAB (Fig. 2I). Similarly, hot etching of PB mesocrystals in the presence of polyvinylpyrrolidone (PVP) can produce hollow particles.[60] In this method, mesocrystals and PVP were strategically chosen to promote the etching inside the particles. In comparison, single PB crystals are defect-free and do not have a high energy grain boundary to let the HCl molecules diffuse inside the particles. Therefore, the etching starts at the surface and creates superficial voids. The role of PVP is to bind with the iron atoms in PB and control the etching rate. A thicker PVP layer inhibits etching, while too little PVP cannot guarantee the uniformity of the hollow particles. Depending on the particle size and temperature, these particles can be transformed upon calcination into different phases of iron oxide.[61] Most PBAs are unstable in basic media. Thus, using bases like NaOH or NH_4OH became common to etch them. Nevertheless, the presence of OH^- can start the simultaneous formation of metal oxide/hydroxide, directly leading to PBDs.[8] Therefore, the concentration, temperature, and/or etching time must be carefully controlled. The use of ammonia has consistently been demonstrated to preferentially etch the corners of the cubic structures of different PBA compositions, indicating a reliable way to form hollow cages.[22–24]

Fig. 2J and K showsan example of nickel hexacyanoferrate (NiHCFe) cages produced by ammonia etching.[23] As the etching depends on defect density, a less crystalline PBA will induce a faster etching rate, leading to over-etching and collapse of the cubes at prolonged etching times.[23] Due to the increased surface area, hollow particles are attractive for improving the performance in applications directly affected by the available surface area and mass diffusion. Consequently, etching has been further developed and utilized with other synthesis conditions,

 This journal is © The Royal Society of Chemistry 2023

Open Access Article. Published on 15 March 2023. Downloaded on 2/9/2026 11:49:42 AM.
This article is licensed under a Creative Commons Attribution 3.0 Unported Licence.

like milder etchants such as urea.[20] The control of the etching rate is a crucial part of tailoring the morphology, producing uniform hollow/porous particles, and avoiding structure collapse during the etching or derivatization step. For added control of the chemical composition of the PBA, etching can also be carried out along with ion exchange.

3.1.3 Ion exchange. The ion exchange process is a solubility- and equilibrium-driven method to modify the PBA chemical composition and comprises two sub-categories of anion and cation exchange. Most of the time, this process also changes the morphology, creating core–shell structures, hollow particles, or other hierarchical structures. Similar to etching, depending on the conditions, ion exchange can also directly lead to PBDs rather than simply modifying PBA characteristics, for example, with NaOH treatments, as will be discussed further.[8] The advantage of the PBA co-precipitation method is that one PBA can be a seed for the growth of a second PBA composition, creating core–shell structures. The difference in solubility of the two phases promotes ion-exchange processes, which can change the morphology by creating yolk–shell or completely hollow materials. The difference in PBA solubility compared to that of other metal salts can also be used to prepare PBA compositions that are normally not stable by direct co-precipitation. For example, cobalt in cobalt hexacyanocobaltate (CoHCCo) can be partially exchanged for Mo by adding MoO_4 to a CoHCCo suspension[22] (Fig. 2N and O). Mo occupies the M–NC sites due to the weaker character of the Co–NC bond compared to that of Co–CN. This site occupancy later plays an essential role in the derivatization process, leading to a hybrid composed of Mo_2N and Co_3O_4. In PBAs, the coordination of the metal to the carbon of cyanide has a much stronger character than the one to nitrogen. Therefore, in many ion-exchange strategies, only the M–NC can be replaced in the original structure. Even in the case of complete dissolution of the PBA to react with the salt additive, the new metal ion will react with the $[M'^{x+}(CN)_6]^{(6-x)-}$ unit, retaining the M′–CN character. Zhang *et al.* combined etching with ion exchange to modify chemical composition while creating porosity.[24] When cubes of nickel hexacyanocobaltate (NiHCCo) are mixed with ammonia, the corners are etched, creating hollow cages. At prolonged times, the etching continues at the edges until the six cube faces are separated, leading to plate-like morphology. If palladium salt is mixed with NiHCCo and ammonia, Pd ions partially replace Ni (as they are coordinated with nitrogen). Interestingly, ion exchange accelerates the morphology change caused by ammonia, directly leading to PdNiHCCo plates rather than hollow cages. Even if the NiHCCo cubes are first etched and then mixed with Pd, hollow cages cannot be accomplished, indicating that ion exchange preferentially takes place at the edges, causing dissolution and collapse of the cubes. A similar cation exchange based on this principle was conducted by synthesizing a more soluble manganese hexacyanoferrate (MnHCFe) and then adding cobalt nitrate that replaced Mn atoms to form CoHCFe in the presence of C_2H_2OH (Fig. 2L and M).[62] Ion-exchange in this way can be regarded as similar to the templating method, and the initial PBA before ion-exchange is regarded as the sacrificial template.

3.1.4 Coating and surface modification. The coating of PBA particles is performed to improve the electrical conductivity of PBDs as most of the derivatives, like metal oxides, or sulfides, have intrinsic low conductivity. As a secondary effect, the coating can also prevent particle aggregation and coarsening during derivatization.[63] Some studies report the successful capitalization of carbon atoms of cyanide ligands as the source to produce conductive carbon within the PBDs.[24] Nevertheless, this is achieved under specific and mild conditions like low temperature (<400 °C) and a N_2 atmosphere, which is unsuitable for most derivatization processes. Therefore, the coating step is usually performed with a carbon precursor that can later be converted into a conductive carbon shell. The coating can be performed by using polymers that bind to the material. This binding ability can be an inherent property of the polymer or has to be facilitated by treating the surface and adding elements that ease the attachment of the coating precursor to the substrate. Two main examples are resorcinol formaldehyde (RF) and polydopamine (PDA).[63–67] RF can be used as a shell on PBA particles to produce core–shell morphology (Fig. 2P and Q). These particles can then be converted to a yolk–shell by heat treatment. A RF resin shell can be implemented on particles by using a surfactant, such as CTAB, that is stabilized on the PB particle surface and promotes the polymerization of resorcinol and formaldehyde.[67] Coating with PDA can be performed in a single step and simultaneously with PBA co-precipitation.[63,65] This is due to the self-polymerization of dopamine hydrochloride through its oxidation in the presence of Fe^{3+} or some other oxidized metals. The polymerization takes place by non-covalent bonding of Fe^{3+} and catechol. The pH of the solution or the presence of oxidative agents further promotes polymerization kinetically and thermodynamically.[65]

A recent study observed that the incorporation of a PDA affected the particle size and material composition. In the synthesis of CuHCFe, the presence of a PDA coating stabilized potassium in the PBA crystal, which subsequently affected the final derivative composition.[63] Electrospinning is also an adopted strategy to cover the PBAs with polymeric carbon precursors. By dispersing the synthesized PBA particles in the spinning solution, fibres of PBAs embedded in a carbon matrix are produced. Upon heat treatment, the particles are converted into the targeted PBD, while the fibres can carbonize and form a network of conductive carbon.[68–70] Besides acting upon conductivity, the PBA surface can be modified or coated with other materials that provide extra elements in the derivatization process. For example, adding thiols to the material can provide a source of sulfur to produce PBD metal sulfides.[71] Anchoring metal precursors can alter the metallic derivative's composition and morphology. For example, CoHCCo cubes are modified with $Ni(OH)_2$, creating a core–shell composition. Upon sulfidation, both materials are converted, creating a CoS_2@NiS_2 hierarchical structure rather than a homogeneous mixture of CoS_2 and NiS_2.[72]

3.1.5 Composites and hybrids. Creating composites or hybrids with other materials that do not necessarily change PBA particles but rather act as a support or active material in PBD

Open Access Article. Published on 15 March 2023. Downloaded on 2/9/2026 11:49:42 AM. This article is licensed under a Creative Commons Attribution 3.0 Unported Licence.

application is one of them. For example, carbon nanotubes (CNT),[73,74] carbon cloth,[75] graphene,[76,77] and nickel foam,[58,78–80] among others, can act as a substrate for particle growth or simply anchoring. In cases where direct anchoring of PB on the substrate is impossible or inefficient, a second substrate can be used. Fig. 2R and S show an example where NiCo arrays were first formed by a hydrothermal procedure on carbon cloth, and then NiHCCo was formed on the arrays.[75] These substrates are rather stable up to high temperatures and do not actively change PBA particles nor modify them upon derivatization. However, they act as a support for a PBD material while improving mechanical and electrical properties. Materials with target properties can also be added that do not necessarily decompose or react during the derivatization process. Wang *et al.* modified the surface of PB cubes with CeO_2 nanoparticles.[81] The modification occurs through a redox reaction between $Ce(OH)^{2+}$, formed due to hydrolysis of hexamethylenetetramine, and Fe(III) species of PB. This mechanism leads to an intimate interaction between the as-produced CeO_2 particles and the PB surface, preventing the aggregation or segregation of the particles during heat treatment.

3.1.6 Other approaches. Simply modifying PBA synthetic conditions can also significantly change the morphology or composition. For example, by varying the ratio between Co^{2+} and $[Fe(CN)_6]^{3-}$ in solution, the morphology of CoHCFe can progress from rounded cubes to nanoframes.[82] At the same time, increased ageing time can lead to hollow particles, which is possibly a greener alternative to the etching methods. Most of the PBA studies rely on co-precipitation. There are alternative synthetic methods for PBA preparation, for example, electrodeposition which can better control particle size, or the hydrothermal method, which can tune porosity. Wang *et al.*[15] controlled manganese hexacyanocobaltate (MnHCCo) morphology and porosity by varying reaction times during hydrothermal processing. The particles evolve from rounded cubes to cross-shaped etched faces.[15] The morphology is then retained upon pyrolysis. In this case, no pre-treatment *per se* is applied, but the PBA synthesis is rationally designed. As previously mentioned, the synthetic routes for controlling PBA composition, growth, and morphology are plenty, and many (if not most) of them remain unexplored for PBD synthesis.[28] The combination of the synthesis routes and parameters with pre-treatment methods gives space for improving the control over PBD morphology and composition and better tuning of their properties.

3.2 Derivatization

We define derivatization as the step in which a PBA is used as a template/precursor and converted into another material. The two widely adopted methods are hydrothermal and thermal syntheses, through which many chemical compositions can be derived. They are usually relatively simple and fast methods with great scalability potential. Liquid methods are far less reported. However, they enable complex compositions and morphologies. The following metallic compounds have been reported as derivatives from PBAs: carbides, oxides, sulfides, fluorides, hydroxides, nitrides, phosphides, phosphosulfides, selenides, and selenophosphides. In addition, metal alloys or pure metals and carbon can be derived from PBAs by extra steps, besides composites or hybrids within these compositions. A primary factor separating each group of compounds is the temperature of the treatment. Because they have different thermal stabilities, one can control the dominant phase by controlling the temperature. Both thermal and hydrothermal treatments can be used for lower-temperature treatments, but only thermal procedures can be conducted for higher temperatures. The final chemistry of the derived compound depends on the environment during derivatization, besides the (pre-treated) PBA composition itself. In thermal treatments, the atmosphere can carry the reactive element, for example, oxygen (in synthetic air or O_2) or nitrogen (in NH_3). It can also be a carrier of the reactive material typically placed upstream in the furnace or mixed with the PBA. The gas can also be an inert component, enabling the synthesis of carbides, for example.

Similarly, additional salts can be placed in the media to promote specific compositions in hydrothermal or liquid methods. For example, by hydrothermal treatment of a Co–Ni PBA with ammonium thiomolybdate, mixed Ni–Co–Mo sulfide can be derived.[83] Here, an overview of the derivatization strategies is provided for each compound group. These procedures are summarized and shown schematically in Fig. 3 and Table 2.

3.2.1 Oxides. These compounds were the first and most widely reported PBDs, as they can be easily prepared through a simple standalone thermal step, or subsequent to hydrothermal, and liquid methods.[8,11,12,22,55–59,61,67,69,81,84–87] During thermal treatment, oxidation can be achieved in open air, synthetic air, or oxygen. To successfully derive metal oxide or mixed metal oxides from PBAs, the temperature and duration of the treatment have to be controlled with precision. A broad range of temperatures from 250 °C to 900 °C can be implemented for oxide derivatization, depending on the desired oxide phase. PB has been extensively investigated to produce iron oxides, given the two iron centres present in its structure. A great compilation focused on PB-derived Fe_xO_y can be found elsewhere.[13] In general, the thermal decomposition of PB enables the stabilization of other phases of Fe_2O_3 rather than α-Fe_2O_3. The crystallinity and resulting phase depend not only on the temperature but also on the PB particle size and morphology. In a multi-step approach, Liu *et al.* reported yolk–shell spheres of Fe_2O_3@C that were further treated to produce sulfides (Fig. 3C).[67] Hu *et al.* prepared hollow PB particles of different sizes based on the PVP method.[60] When calcined at 250 °C, the smaller particles (110 nm) led to a mixture of amorphous and γ-Fe_2O_3, while the larger ones (190 nm) resulted in the γ-phase only.[61] Similarly, when calcined at 400 °C, the large particles oxidized into single α-Fe_2O_3 while the smaller ones were composed of a mixture of α- and γ-Fe_2O_3. In addition, if standard non-hollow small PB cubes (110 nm) are heat-treated, no crystallinity is achieved even at 400 °C. This indicates that the smaller the surface area, the slower the crystallization and conversion. When different metals are present in the structure, more complexity is added to the oxidation of PBAs. Since most metals have a high oxygen affinity, homogeneous

 This journal is © The Royal Society of Chemistry 2023

Open Access Article. Published on 15 March 2023. Downloaded on 2/9/2026 11:49:42 AM.
This article is licensed under a Creative Commons Attribution 3.0 Unported Licence.

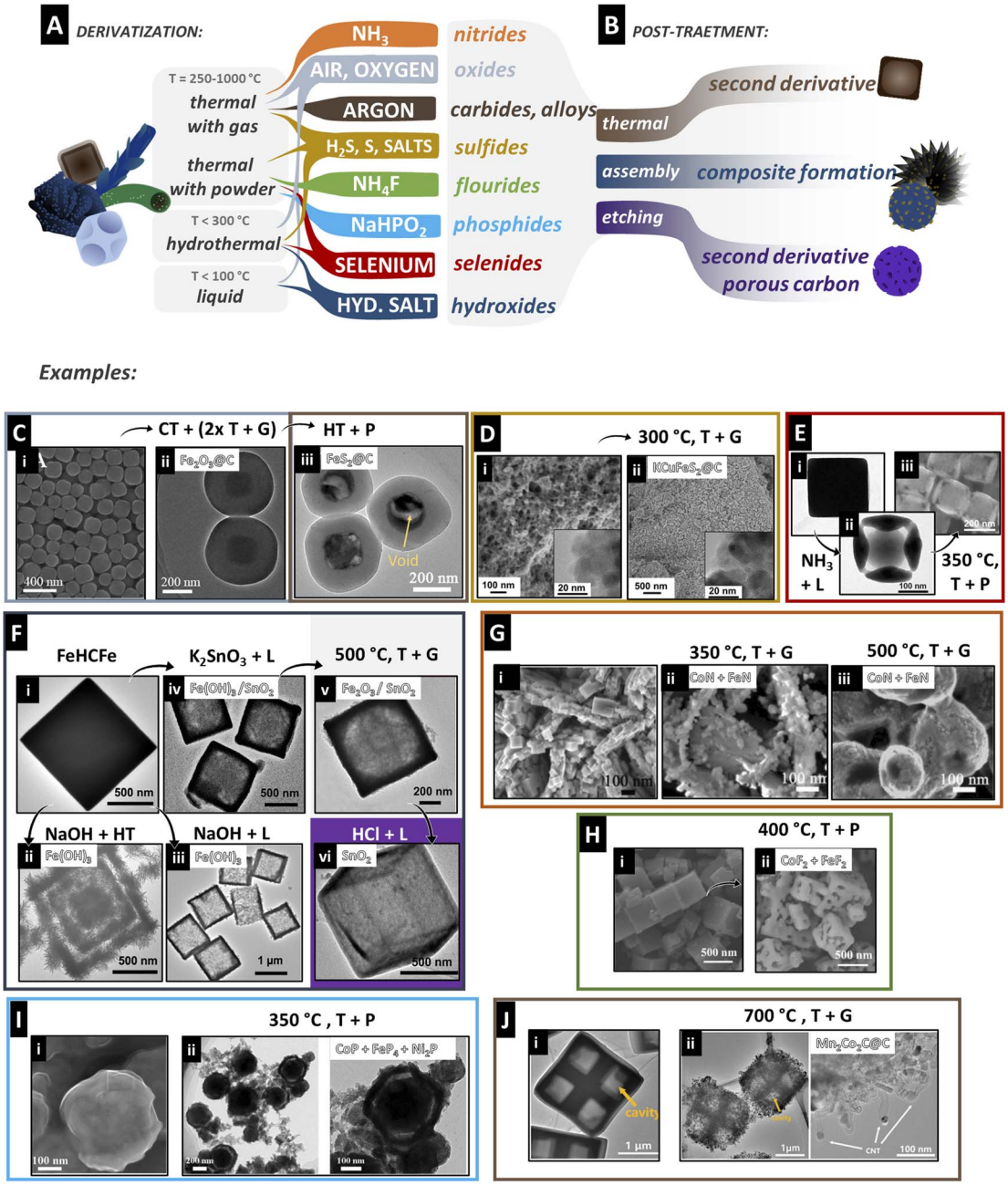

CT: coating, T+P: Thermal+powder, T+G: thermal with gas, HT: Hydrothermal, L: liquid.

Fig. 3 (A and B) Overview of typical compounds derived from PBAs and the common route for derivatization. (C) Consecutive treatments of PB to obtain FeS_2@C yolk–shell structures. Coating with resorcinol followed by 2-step annealing leads to a Fe_2O_3@C yolk–shell (ii). Further hydrothermal treatment with thioacetamide leads to the final derivative. Reproduced with permission of ref. [67]. Copyright 2019 American Chemical Society. (D) Carbon-coated mixed metal sulfide nanoparticles obtained by thermal treatment in H_2S/Ar gas. Reproduced with permission of ref. [63]. Copyright 2022 American Chemical Society. (E) Cages of mixed selenides obtained through etching with ammonia solution (ii) followed by thermal treatment with Se powder in N_2. Reproduced with permission of ref. [23]. Copyright 2017 WILEY-VCH Verlag GmbH & Co. KGaA, Weinheim. (F) Several derivatives obtained from PB by different methods: (ii and iii) treatment with NaOH produces multi-shelled (ii) or hollow (iii) metal hydroxide cubes with hydrothermal treatment (ii) or in room temperature solution (iii). (iv) New metals can be incorporated by the dissociation of metal oxide salts and form partially hollow cubes of hydroxide/oxide mixtures that can be heat treated in air to form oxides (v) and further etched with acid to remove one phase (vi) creating single metal oxide hollow cubes. Reproduced with permission of ref. [8]. Copyright 2013 American Chemical Society (G) Hierarchical metal nitrides coated on Ni foam/$Co(OH)_2$ obtained by thermal treatment with NH_3. The higher the temperature, the more coarsening occurs (ii and iii). Reproduced with permission of ref. [58]. Copyright 2018 WILEY-VCH Verlag GmbH & Co. KGaA, Weinheim. (H) Porous cubes of metal fluoride mixtures directly obtained from thermal treatment with NH_4F in argon. Reproduced with permission of ref. [21]. Copyright 2019 Elsevier B.V. (I) Ternary mixed metal phosphide core–shell particles are obtained by annealing with NaH_2PO_2 in N_2. Reproduced with permission of ref. [102]. Copyright 2021 American Chemical Society. (J) Porous hollow cross-shaped frames of mixed metal carbide@carbon nanotubes obtained by direct annealing of the PBA in Ar. Reproduced with permission of ref. [15]. Copyright 2020 Wiley-VCH GmbH. CT: coating, T + P: thermal + powder, T + G: thermal with gas, HT: hydrothermal, L: liquid.

Open Access Article. Published on 15 March 2023. Downloaded on 2/9/2026 11:49:42 AM.
This article is licensed under a Creative Commons Attribution 3.0 Unported Licence.

Table 2 Examples of the PBA derivatization process and application of the resulting PBD[c]

PBA, morphology	Pre-treatment (method)[a,b], conditions. morphology	Derivatization (method)[b], conditions, morphology	Post-treatment	PBD	Application	Ref
NiTCNi, nanoplates		(T + P), NaH_2PO_2, Ar, 300 °C, 2 h, porous nanoplates		Ni_5P_4 + Ni_2P + C	OER	105
		(L) 2 M NaOH, RT, 10 min, amorphous porous nanoplates		$Ni(OH)_2$	OER	
		(T + G), air, 300 °C, 1 h, porous nanoplates		NiO	OER	
CoHCFe, cubes	(ET + HT), urea, frames	(T + P) NaH_2PO_2, N_2, 300 °C, 2 h, porous nanoframes		$Co_{0.6}Fe_{0.4}P$ + C + N	HER and OER	20
CoHCCo, cubes	(CT + L), $Ni(NO_3)_2$ + urea, core–shell	(T + P), thiourea, N_2, 350 °C, 2 h, core–shell		CoS_2@NiS_2	Capacitor	72
FeHCFe, cubes	(ET + HT), 0.2 M NaOH, hollow box	(T + G), air, 300 °C, 6 h, hollow box		α-Fe_2O_3	Li-ion battery	8
	(ET), RT, 0.2 M NaOH, yolk–shell porous box	(T + G), air, 300 °C, 6 h, yolk–shell porous box		α-Fe_2O_3		
	(ET + IE), $K_2SnO_3 \cdot 3H_2O$, $Fe(OH)_3$/SnO_2 hollow box	(T + G), air, 500 °C, 6 h, α-Fe_2O_3/SnO_2 hollow box	HCl etching	SnO_2, porous hollow box	Li-ion battery	
NiHCCo, cubes	(TP), electrospinning nanofibers	(T + G), air, 200 °C, 2 h, nanofibers	Thermal annealing 800 °C, Ar/H_2	NiCo alloy@C	OER	16
NiHCCo, cubes	(ET + IE), $(NH_4)_2S$, hierarchical microspheres	(T + P), sulfur, N_2, 350 °C, 2 h, hierarchical microspheres		NiS_2	Solar cells	94
NiHCCo, cubes	(CT), PDA, core–shell	(T + G) Ar, 600 °C, 2 h, hollow nanocages		NiCo + C	Li–S battery	65
		(T + P) NaH_2PO_2, Ar, 400 °C, 2 h, hollow nanocages		NiCoP + C		
CoHCFe, cubes on $Co(OH)_2$ sheets		(T + G) air, 450 °C, 2 h, cubes		Co_3O_4 + Fe_3O_4	OER and HER	58
		(T + G) NH_3, 450 °C, 2 h, cubes		$Co_{5.47}N$ + Fe_3N		
FeHCFe, cubes	(CT + ET), resorcinol, urea, core–shell	(T + G, HT) Ar, 150 °C, 2 h, 600 C, 2 h, yolk–shell Fe_2O_3@C	Hydrothermal, TAA, 160 °C, 20 h	FeS_2@C	Li-ion battery	67

[a] ET: etching, IE: ion exchange, CT: coating, and TP: template. [b] T + P: thermal + powder, T + G: thermal with gas, HT: hydrothermal, and L: liquid. [c] CoHCFe: cobalt hexacyanoferrate. FeHCFe: iron hexacyanoferrate (PB). HER: hydrogen evolution reaction. NiHCCo: nickel hexacyanocobaltate. NiTCNi: $Ni(H_2O)_2[Ni(CN)_4] \cdot xH_2O$. OER: oxygen evolution reaction. RT: room temperature. and (TAA): thioacetamide.

This journal is © The Royal Society of Chemistry 2023

Open Access Article. Published on 15 March 2023. Downloaded on 2/9/2026 11:49:42 AM. This article is licensed under a Creative Commons Attribution 3.0 Unported Licence.

derivatization might not occur at low temperatures anda short derivatization time. This might result in mixtures of single-metal oxides over mixed-metal oxides due to a higher oxygen affinity of one of the metallic species. For example, upon oxidation of CoHCFe nanoframes at 350 °C for 2 h, the resulting oxide is composed of a mixture of Co_3O_4, $CoFe_2O_4$, and K_2CoO_3.[56] Meanwhile, oxidation of hollow nanocubes and nanospheres of CoHCFe at 500 °C for 3 h led to a single phase of $Fe_yCo_xO_4$.[55] Phase diagrams can be used as an estimation guide while reducing the strength of oxidation by decreasing the synthetic air-to-argon ratio or using carbon dioxide gas can help to achieve better control over oxidation. Li *et al.* reported a copolymer-co-morphology synthetic strategy to prepare spinel oxides, where metal ratios initially tuned the composition of the oxide in the PBA.[11] In this approach, Mn–Fe hexacyanocobaltate ($Mn_yFe_{1-y}HCCo$) with different Mn/Fe ratios is prepared by simultaneous addition of $FeCl_2$ and $Mn(NO_3)_2$ to $K_3[Co(CN)_6]$. When heat-treated at 500 °C for 1 h, spinel $Mn_xFe_{1.8-x}Co_{1.2}O_4$ ($0 < x < 1.8$) hollow nano-dice are obtained. Besides tuning the composition, the decrease in the Mn content leads to a morphological progression from cubes to spheres, demonstrating that the chemical composition also plays a role in morphology control. In terms of morphology, shrinkage of PBA particle is normally reported when being oxidized due to the removal of the CN units. This is followed by an overall increase in surface roughness and surface area, which is desired in many applications. Though many studies report a direct templating of PBA into PBDs, that is, changing the composition but retaining the original PBA morphology, that is not always the case. Zhang *et al.* demonstrated the morphological evolution of PB cubes at different treatment temperatures.[85] When crystalline PB cubes of 1 μm are heat treated at 350 °C, the outer part of the cubes is oxidized, while the centre atoms diffuse outwards, creating a Fe_2O_3 shell-microbox. When the temperature is increased to 550 °C, there is particle coarsening, resulting in porous hollow microboxes, which further progress to a hierarchical structure of hollow boxes composed of Fe_2O_3 nanoplates at 650 °C. This shows that even in the absence of pre-treatments, hollowness and morphology can be tuned with heat treatment parameters. Hollowness in PBA particles through heat treatment has been explored for other compositions as well. This is achieved through the Kirkendall effect, where the difference in the diffusion of the metals, or the metals and the gas, leads to internal voids in the PBD particles. If well controlled, morphologies like yolk–shell can be achieved.[88]

Though less explored, liquid methods are also used for deriving PBA into oxides. However, this is achieved by the initial derivatization of PBA into hydroxides and further thermal treatment of PBD–OH. Therefore, the liquid approaches will be discussed in the hydroxide section.

3.2.2 Sulfides and selenides. Derivatization of PBA to these chalcogenides can be performed by both hydrothermal and thermal procedures, while sulfides have also been achieved by liquid methods.[23,67,71,72,75,76,83,89,90] In the thermal method, H_2S can be directly used, or sulfur powder can be heated to produce sulfur vapour and combined with H_2 gas to diffuse as H_2S gas in the PBA structure. Sometimes sulfur or sulfur-containing additives are incorporated in the PBA particles in pre-treatment steps, acting as a source of sulfur during the heat treatment.[71] Similar procedures can be performed by putting selenium powder in the upstream side of the furnace or simply mixing the ground powder with other reactants. Temperatures between 300 and 500 °C usually provide the necessary energy for the formation of homogeneous chalcogenides.[72,75] Nevertheless, partial sulfidation/selenization through thermal methods is more difficult to control, normally resulting in complete conversion of the treated materials.[63,71]

Bornamehr *et al.* were able to completely convert CuHCFe into chalcopyrite within only 10 minutes of treatment at 300 °C with H_2S gas.[63] In this work, the authors demonstrated the effect of the coating on the derivative composition. The polydopamine used to coat and control the particle size also led to a potassium-rich and less defective CuHCFe phase. As a result, the sulfide derived from the coated material was $KCuFeS_2$, while for the uncoated, it was $CuFeS_2$ (Fig. 3D). This work also presents significantly smaller derivative particles (<100 nm) than the usual 0.5–2 μm range. Higher surface area can be achieved with smaller particles; however, it is more difficult to incorporate morphology complexity in this size range.

In the hydrothermal procedure, a sulfur-containing compound such as the Na_2S salt or thioacetamide can release S^{2-} anions and promote anion exchange in the PB lattice to form metal sulfide.[67,91] For selenides, the selenium powder can be dissolved in water to use as the reactive environment in hydrothermal methods.[92] Reaction temperatures for forming metal chalcogenides in hydrothermal synthesis are reported between 120 and 200 °C. However, the product of hydrothermal synthesis is often subjected to a subsequent thermal annealing process to achieve complete conversion and crystallinity. Liu *et al.* reported an interesting multi-step procedure to prepare yolk–shell spheres of FeS_2@C derived from PB (Fig. 3C).[67] Initially, PB particles are coated with a resorcinol–formaldehyde resin (RF). Upon two-step annealing in Ar at 150 °C and 600 °C, the PB particles shrink and oxidize to Fe_2O_3 while the RF coating graphitizes into a carbon shell, forming a yolk–shell structure. The spheres were modified with thioacetamide, and through hydrothermal synthesis at 160 °C, FeS_2@C yolk–shell particles were achieved. The coating prevents agglomeration and coarsening of particles, while annealing at higher temperatures is essential to achieve conductivity in the formed carbon shell. Another way to achieve sulfides with yolk–shell morphology is through the Kirkendall mechanism and ion exchange. This was performed, for example, by reacting cadmium hexacyanoferrate (CdHCFe) with Na_2S at 150 °C under 10 atm.[93] The S^{2-} ions are exchanged with $[Fe(CN)_6]^{3-}$, forming CdS. As the Cd^{2+} ions diffuse outwards faster than S^{2-} can diffuse inwards, hollowness starts to appear between the surface and the centre of the cubes, resulting in a CdS yolk–shell structure. When NiHCCo is reacted with Na_2S at 100 °C, the cube faces are etched first, and the morphology evolves to NiS_x nanocages rather than yolk–shell structures.[91] Using $(NH_4)S$ instead of Na_2S drastically changes the morphology. Huang *et al.* prepared hierarchical NiS_2 particles by treating NiHCCo cubes with $(NH_4)S$ by the hydrothermal method at 100 °C.[94]

Open Access Article. Published on 15 March 2023. Downloaded on 2/9/2026 11:49:42 AM. This article is licensed under a Creative Commons Attribution 3.0 Unported Licence.

Through hydrolysis, OH^- and S_x^- are formed, and OH^- slowly etches the Ni^+ ions, leading to γ-NiOOH. At prolonged times, NiHCCo cubes are completely dissolved, and γ-NiOOH is partially converted to NiS_x while the morphology evolves to hierarchical microspheres of γ-NiOOH/NiS_x. These particles are crystallized and converted to NiS_2 by thermal treatment at 350 °C with sublimed sulfur powder. These last studies are the few examples where the metal from the $[M'(CN)_6]$ unit is completely removed from the final derivative, as no iron[93] or cobalt[91,94] remains in the material. Nai *et al.* also utilized ammonia to prepare cages of NiHCFe,[23] by heat treatment with Se powder at 350 °C, obtaining a mixture of $NiSe_2$ and $FeSe_2$ (Fig. 3E). Like oxides, obtaining mixed metal chalcogenides rather than a mixture of single metal components also requires careful tuning of derivatization parameters. Selenide powder was also used as a post-treatment to dope $(CoFe)S_2$.[95] Hollow cubes of CoHCFe were prepared in the presence of trisodium citrate and then mixed with sulfur powder. After heat treatment at 350 °C for 2 h, $(CoFe)S_2$ is formed. Mixing the sulfide with selenium powder and treating it at 250 °C for 8 h leads to the Se-doped $(CoFe)S_2$ hollow boxes. The inverse process, first selenization followed by sulfidation was also performed, resulting in S-$(CoFe)Se_2$.

3.2.3 Hydroxides. The conversion of PBAs into hydroxides can be realized through liquid and hydrothermal procedures.[8,58,94] Perhaps the most extensive example is the work by Zhang *et al.*[8] In this work, PB cubes were transformed into different hollow and hierarchical cubes with different compositions driven by basic etching and ion exchange. In the presence of NaOH solutions, PB is converted to $Fe(OH)_3$. The morphology of the resulting cubes depends on the NaOH concentration and temperature, generating yolk–shell, hollow cubes, or multi-shelled microboxes (Fig. 3F(ii) and (iii)). In the presence of MOx salts ($K_2SnO_3{\cdot}3H_2O$, Na_2SiO_3, Na_2GeO_3, $NaAlO_2$, or $NaBO_2{\cdot}4H_2O$), basic etching from salt hydrolysis and ion exchange takes place, resulting in homogeneous $Fe(OH)_3/MO_x$ hollow cubes (Fig. 3F(iv)). Upon annealing, they can be converted into mixtures of Fe_2O_3 and MO_x (SnO_2, SiO_2, GeO_2, *etc.*) and further single MO_x hollow cubes by etching out the Fe_2O_3 phase (Fig. 3F(v) and (vi)). This work demonstrates the versatility of changing morphology and composition by finely tuning reaction parameters.

As discussed in the sulfide section, $(NH_4)S_2$ can also go through hydrolysis, producing NH_3 and H_2S which are decomposed into OH^- and S_x^{2-}.[94] This leads to a simultaneous transformation of the PBA into oxyhydroxide and partial sulfidation with a complex morphology evolution. In general, the use of a metal salt rather than a strong base or ammonia leads to slower and more controlled derivatization into hydroxide. This is also a pathway to introduce new elements to the PBA/PBD structure, especially if they do not typically form stable PBA complexes, like Ge, Si, Al, and B in the work of Zhang *et al.*[8] This strategy was also used by Hu *et al.* to form oxide mixtures of Fe and W.[96] By stirring PB cubes with Na_2WO_4 at 50 °C, $Fe(OH)_3/WO_{3-x}$ hollow cages are formed. Through calcination at 550 °C for 6 h, $Fe_2O_3/W_{18}O_{49}$ composites are then obtained. The liquid methods allow the synthesis of more complex or hierarchical structures, which is usually not the case for thermal treatments. Therefore, PBD–OH is typically used as a precursor for other PBD compositions like PBD-oxides, instead of direct oxidation of PBAs, and PBD-sulfides, by heat treatment with sulfur powder.[94]

3.2.4 Fluorides and nitrides. These compounds remain little explored and are mainly synthesized by thermal procedures. For nitrides, derivatization can be achieved with the aid of NH_3 gas.[58,97] Some studies capitalized on the nitrogen from CN ligands and prepared metal nitrides as well.[22] Nevertheless, most commonly, nitrogen from CN is either removed or results in N-doped carbon rather than metal nitrides. Of the few reports on nitrides, the majority covers the conversion of PB into Fe_2N, and most metals/compositions are still to be studied.[97,98] Wang *et al.* demonstrated that under an NH_3 flow, CoHCFe templated over $Co(OH)_2$/nickel foam is converted into a mixture of FeN and CoN.[58] At a lower temperature (325 °C), interconnected nanosheets are obtained. When the temperature increases to 350 °C, 450 °C, and 500 °C, coarsening and coalescence occur, resulting in complete loss of the initial nanostructure (Fig. 3G). The higher the temperature, the less nitrogen is incorporated into the material, resulting in mixtures of nitrides with different stoichiometric ratios. Wang *et al.* described the formation of FeCoNiN on nickel foam (NF) by treatment of CoHCFe/$Ni(OH)_2$/NF with ammonia. However, the large amount of Ni suppresses more structural and composition insights into Co- and Fe-derived components, with evidence of Ni_3N.[99] Fluoride-based PBDs are also quite limited, though more restricted in terms of synthetic approaches, given the toxicity and hazards of fluorinated compounds, especially at high temperatures. One report uses the templating approach to grow NiHCFe onto $Ni(OH)_2$@Ni foam nanosheets.[79] This material is then fluorinated by a thermal process through the decomposition of NH_4F at 350 °C for 2 h and the effect of the NH_4F ratio and temperature were evaluated. They show that fluorine suppresses the release and decomposition of CN units, producing a more stable hierarchical structure compared to that of the same sample annealed in argon. Fluorination results in F-doped NiFeOOH rather than a fluoride compound. Nevertheless, F-doping plays an important role in the catalytic activity of the material. Differently, when bare CoHCFe cubes are heat treated at 400 °C with NH_4F, etched porous cubes of CoF_2 and FeF_2 mixtures are formed (Fig. 3H),[21] indicating that Co/Fe mixtures might be more prone to fluorination than Ni/Fe.

3.2.5 Phosphides and phosphor-containing compounds. Due to their high hydrogen evolution activity as catalyst and their low cost as opposed to the noble metals, different phosphor-containing compounds have been investigated as PBDs, being the emerging PBD class of compounds after the pioneering oxides.[20,64,65,74,75,77,78,80,82,100,101] Metal phosphides are derived by a thermal procedure using NaH_2PO_2 powder under an inert gas flow such as Ar or N_2. Similar to selenization and sulfidation, the powder can be mixed with the reactants or placed on the upstream side of the tube.[20,65] Zhou *et al.*[102] prepared mixtures of 3 different phosphides by treating FeHCCo with $NiCl_2$ to form NiFeHCCo, and further heat treatment with NaH_2PO_2 in N_2. The heating leads to a core–shell

Open Access Article. Published on 15 March 2023. Downloaded on 2/9/2026 11:49:42 AM.
This article is licensed under a Creative Commons Attribution 3.0 Unported Licence.

structure that could be related to the higher concentration of Ni at the surface (Fig. 3I). As observed for the derived-oxides, the PBA composition also affects the morphology of the derived phosphide. Ding *et al.* prepared CoHCFe, NiHCFe, and MnHCFe by co-precipitation and phosphorized them under the same conditions (400 °C, Ar, and NaH_2PO_2). After the heat treatment, all materials present a rough surface. However, NiFe–P shows higher particle coarsening while MnFe–P presents small particles adhered to the cubes.[101] The addition of Se or S powder can result in the formation of selenophosphide or phosphosulfides.[75,89] Similar to other thermal treatments, a temperature range of 300–500 °C has shown the best resulting products in terms of homogeneity. For example, Liu *et al.* performed sulfidation, phosphorization, and phosphosulfidation of NiHCFe, to evaluate the effect of time and temperature on the composition and morphology.[89] At 350 °C and under a N_2 flow in the presence of both sulfur and NaH_2PO_2, the cubic morphology evolves to smaller nanosheets after 1 h of annealing, leading to a complete loss of the cubic shape and morphing into nanoflowers after 2.5 h. The flower morphology is not obtained in the absence of either sulfur or NaH_2PO_2, and only deformed and shrunk cubes are produced. Analysis of composition indicates that the flowers are mixed metal phosphosulfide $(NiFe)PS_3$ rather than individual phosphosulfides. In another phosphide derivatization, similar to the RF strategy, NiHCCo 450 nm cubes were coated by dopamine through the self-polymerization process prior to derivatization.[65] The material was first annealed at 600 °C to ensure carbonization of the coating while forming a Ni–Co alloy. This results in carbon-coated NiCo hollow cubes. The PBD was then treated with NaH_2PO_2 at 400 °C to convert the alloy into a mixed NiCo phosphide. Jiang *et al.* also utilized dopamine for PBD preparation. They demonstrated a tubular PB morphology rather than the usual cubes.[64] After coating tubular PB particles with dopamine, the material was converted to carbon-coated FeP. They used the original PB as a cathode and the PBD FeP as an anode in a sodium-ion battery full cell. In many cases, the PBAs are combined with carbon structures prior to the phosphorization process.[65,74,77] The carbon structures, like carbon nanotubes and graphene, enhance the overall electronic conductivity of the derivative and anchor the PBD particles, demonstrating improved catalytic performances compared to the bare PBD.[77]

3.2.6 Alloys, carbides, and carbon. By heating the PBAs in an inert atmosphere such as Ar, without providing other elements, alloys and metal carbides can be obtained.[13–17,24,62,65,68,70,84,103,104] For example, the treatment parameters used for oxidation in air can be replicated under Ar to produce a metallic alloy/carbon composite.[84] While mild conditions will form alloys and carbon mixtures, the formation of carbides requires higher temperatures (>500 °C). This can make it challenging to achieve carbides with different morphological features like high porosity and hollowness. As demonstrated by Wang *et al.*, highly porous cages of MnHCCo can be prepared through prolonged reaction times (Fig. 3J).[15] Nevertheless, when annealed at 700 °C for 2 h, the structures with higher hollowness degrees collapsed. The presence of metal and carbon at high temperatures and under inert conditions can also favour the growth of by-products like carbon nanotubes, affecting the final morphology of the PBD product.[15] After the derivatization of the metal carbide or alloy/C mixture, porous carbon can be produced through a subsequent etching of the metallic species, for example, by using HF or HCl. This carbon material with high porosity can be very attractive for absorption applications.[103,104]

3.3 Post-processing

Some PBD synthesis methods involve post-processing steps to reach the desired product quality and characteristics. This can be liquid etching to remove impurities or additives, such as removing metals in the derivative to produce porous carbon.[103] Simultaneous with etching, more intricate morphologies can be achieved due to ion exchange.[8] Etching can also be utilized as a post-processing step that removes unwanted phases. For instance, if two oxide phases are formed after derivatization, and one is undesired or detrimental to the performance, it can be selectively etched. It also causes *in situ* porosity formation that can be beneficial to the target product.[86] Post-processing can also be in the form of mono- or multi-stage annealing, resulting in higher hybridization and graphitization degrees or higher crystallinity of the PBD phases. The PBD particles can be further incorporated into other materials, for example, within MXene layers, to form MXene/PBD composites.[87] Though they do not fundamentally relate to the PBA derivatization process, these steps affect the resulting PBD composite properties for their target application.

4. PBD properties: structure design and applications

Understanding the structure/property correlation is a key step to enabling PBD use for different applications. Therefore, the derivatization procedure's steps are often engineered to achieve a specific structure. The structure design can be reviewed from two perspectives: first, the elaboration on the PBD synthesis route in each step of pre-treatment, derivatization, and post-treatment; and second, the formation of hybrids and composites by assembling PBAs and other components together. The result of these design strategies is either a final sophisticated morphology such as hierarchical and multi-walled structures that aid the material with improved surface area, mechanical properties, and other characteristics that are beneficial to the final application, or in a chemical composition that improves conductivity, magnetic properties, *etc.* Since each chemical group (carbides, phosphides, oxides, *etc.*) have a diverse effect on performance, the effect of composition can be studied for a particular application, as described in previous revisions.[6,9,10,25,26] Here, attention will be focused on the effect of morphology on the properties and applications.

4.1 Structure design and PBD characteristics

Pre-treatment usually has a crucial effect on the structure design, mainly when etching and ion exchange are employed. For example, by using PVP or citrate, crystal growth can be

Open Access Article. Published on 15 March 2023. Downloaded on 2/9/2026 11:49:42 AM. This article is licensed under a Creative Commons Attribution 3.0 Unported Licence.

controlled to result in a frame or box morphology.[57] The derivatization step can heavily influence the PBD structure.[84,105] Sometimes, due to different precursors (sulfur, selenium, or NaH_2PO_2 powder) and different growth mechanisms of the derivative crystals, the same structure evolves into different morphologies.[19,89] Heat-treatment parameters can also affect the design. It has been shown that treating PBA particles under the same atmosphere but with different temperatures can result in different oxide morphologies.[85]

Besides the synthesis parameters, even morphological attributes such as the cavity size in the PBA can affect the subsequent derivative morphology. This has been shown for different iron oxide phases derived from PB cages with different cavity sizes under the same derivatization parameters.[61] Particle sizes start from around 200 nm when designing more complex and hierarchical structures. The morphology of smaller particles is usually limited to dense cubic shapes that are not well developed and grown. Smaller particles are more prone to collapse when inducing hollowness and porosity and do not provide the necessary volume for morphology design. Furthermore, methods to modify particle morphology rely on protecting specific planes/surfaces and/or attacks on reactive sites. This requires well-structured particles with high crystallinity. The high surface energy of smaller particles makes it more difficult to control and guide morphology changes.

While the elemental composition of PBDs can be relatively easy to control, the resulting phases and stoichiometry rely on many kinetic and thermodynamic aspects of the derivatization process. A key aspect of PBA composition is the relatively limited amount of stable metallocyanide salts, typically varying between $[Fe^{II/III}(CN)_6]^{4-/3-}$ and $[Co(CN)_6]^{3-}$, sometimes $[Mn(CN)_6]^{3-}$ or $[Ru(CN)_6]^{4-}$, though the latter is quite cost-prohibitive. Therefore, most PBA compositions consist of M $[M'(CN)_6]$ with M′ = Fe, Co, Mn, and sometimes Ru. Even though the M element could vary through a large portion of transition metals, nearly all studies report on PBAs with M = Fe, Co, Ni, and Mn. A few examples of alternative metals already reported – though not all for PBD synthesis – are Cu, V, Mg, Zn, Cd, Ag, Ti, Pd, and Mo (Fig. 5). Mixing different M units has become one strategy to increase composition complexity or stabilize different metals in the lattice that would not form a standalone PBA, where even a high entropy PBA with 5 different M is described.[11,106] In principle, mixing different $[M'(CN)_6]^{6-x}$ units are also possible and has been successfully reported.[107] However, the versatility remains limited. Besides, the M unit can be more easily replaced in the structure in pre-treatment procedures like ion exchange due to the lower M–NC bonding strength, providing more flexibility in composition design. The composition of the PBDs will be modified in the derivatization process by incorporating, for example, O, S, or P, and eliminating N and C from the ligands while retaining the metal species (in the absence of post-treatment). Therefore, to some extent, it is possible to predict probable chemical components of PBDs. Nevertheless, the derivatization parameters and morphological features of the PBA precursor will affect the resulting phases. Higher porosity and hollowness provide a larger surface area that can accelerate the conversion or facilitate the diffusion of the metallic species, resulting in different phases or segregation of components, for example, metal oxides *versus* mixed metal oxides.[55,56,61]

Though not covered in this review, the PBA synthetic strategy presents many possibilities for altering morphology and composition. Most of the examples presented here involve the synthesis of PBA by co-precipitation and further modifying the surface, morphology, or composition through pre-treatment and derivatization. The synthesis parameters in co-precipitation can also be tuned to change morphology, like the solvent (H_2O, ethanol), temperature, pH or M/M′ concentration ratio. A few template strategies utilize different materials as the support for PBA nucleation, directing the 3D macrostructure,[58,79,108] or as a support and metallic source, where the template itself reacts with the metallocyanide salt to form a PBA, creating better interaction between the template and PBA.[109] Nevertheless, other synthesis methods and processings exist. One approach involves the single-precursor synthesis through the decomposition of $[M'(CN)_6]$ salt, either by acid-induced or hydrothermal methods.[110,111] This enables the slow release of M′ ions, creating highly crystalline nanoparticles below the 100 nm range, though M = M′ limits the composition. Electrodeposition has the same controlled nucleation and growth effect but allows for a more varied composition (M ≠ M′), especially if the M source is immobilized in the electrode.[112–114] Electrodeposition can also orient the morphology[115] and create PBA composites with the electrode material, for example, carbon nanotubes[112] or graphene.[116] Layer-by-layer assembly is another method for controlled orientation of PBA particles while modifying the surface with potential active materials for derivatization, like polymers (for carbonization and conductivity), thiols or amides (for sulfides or N-doped materials), or nanoparticles (for an additional metallic source and compositional complexity).[80,117,118] Though carbon coating through surface modification is the standard strategy to induce conductivity while avoiding particle aggregation, there are other ways to achieve that, such as electrospinning. Electrospun carbon fibers provide high porosity, conductivity, and specific surface area. PBA particles can be assembled inside the electrospun fibers by electrospinning the PBA particles[16,68,69] or anchoring the particles on the electrospun carbon fibers.[100] After derivatization, the carbonized fibers act as a conductive matrix for the PBD while providing flexibility and mechanical stability.

4.2 PBD morphology and applications

The applications of PBDs are varied since they can present many compositions. The most attention is given to electrochemical applications such as catalysis, energy storage, and conversion. The effect of properties on the application can be discussed from two viewpoints, namely, the effect of chemical composition and the effect of structure and morphology. The chemical composition results from the used precursor and the media chosen for derivatization. This is usually better controlled and easily tailored, though unpredicted or secondary phases can be formed during the derivatization. The unwanted phases can be

 This journal is © The Royal Society of Chemistry 2023

Open Access Article. Published on 15 March 2023. Downloaded on 2/9/2026 11:49:42 AM.
This article is licensed under a Creative Commons Attribution 3.0 Unported Licence.

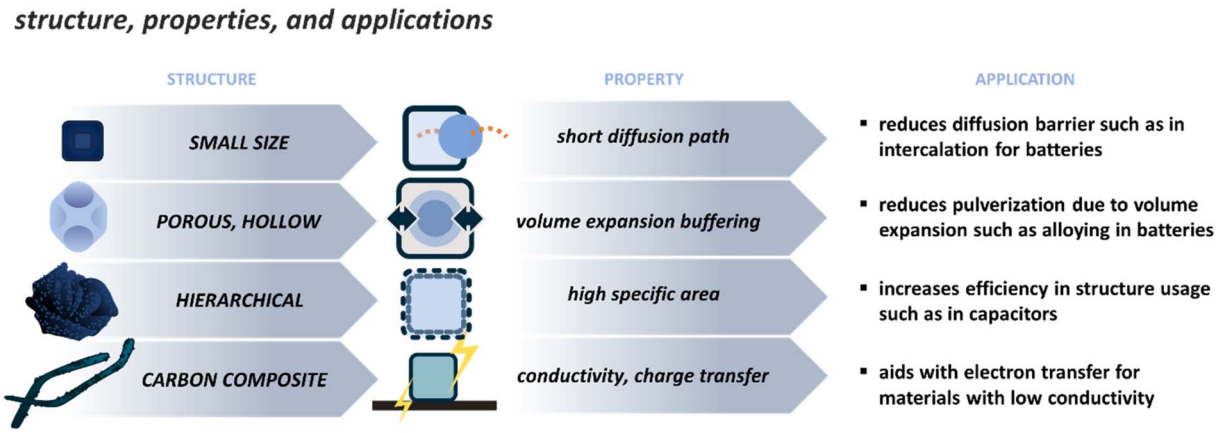

Fig. 4 Main strategies to tune the structure of PBDs, their resulting properties, and examples in applications that are affected by such strategies.

controlled by changing processing parameters or etching the extra phases as a post-treatment step. The chemical composition will have different effects depending on the application, as the target properties will vary. Therefore, here the properties and their effect on the application are focused on the morphology since there are similar morphological features that are beneficial to different applications, for example, tailoring the structure for smaller particle size to reduce the diffusion paths and increase the reaction rate. Typical morphological features are depicted in Fig. 4, and some examples are addressed in Table 2. These standard features can be divided into the following.

4.2.1 Small particle size. Decreasing the particle size is the most common approach to enhance properties, especially in electrochemical applications. This is a rather simple step that enhances electron transfer and element diffusion by reducing the diffusion paths. This method is extensively explored in the PBA application. It uses the synthesis parameters, such as the salt concentration during co-precipitation or the pH to control the growth of the nuclei. A careful treatment keeps the small size attribute of the template. Therefore, studies on the derivatization of the PBA usually do not focus on the effect of the derivative particle size on the properties but rather use strategies in the pre-treatment step to control the PBA size. Li *et al.*[13] provided an overview of PB derivatives and the effect of temperature and environment on the particle size and phase change, and their application in energy storage and conversion. By cross-comparing different reported studies, they showed that a larger particle size usually results in higher crystallinity due to smaller surface area and defects. The effect of particle shape can also be observed in parallel to the size effect. For example, a nanosphere morphology can provide better mechanical stability than a nano-cubic structure and enhance the stability during the cycling of a battery electrode. However, with the same diameter, a cubic structure provides a higher surface area. Liu *et al.*[55] prepared porous nanospheres and nanocubes of iron–cobalt oxide. With the similar size of both morphologies, the spheres provided higher capacity and stability when tested as a lithium-ion battery anode material compared to the cubes due to the higher cobalt loading and better porosity achieved during the processing.

4.2.2 Hollow and porous structures. This method benefits applications that rely on high surface area and fast diffusion. Nevertheless, such properties can also be achieved by reducing the particle size or through sheet morphologies. Their ability to buffer volume expansions in applications where redox and conversion reactions occur makes hollow structures characteristic and attractive. The most prominent example is metal-ion batteries, which rely on the diffusion of ions (like lithium or sodium) into and out of the particles in each charge and discharge step. Depending on the material, alloying reactions can also be part of the charge storage mechanism, which presents a much more significant volumetric expansion (100–400%). Zhang *et al.*[8] provided extensive work on hollow metal oxide boxes. They compared the effect of box layers on the stability of the material as an electrode for Li-ion batteries. A higher number of box layers showed better cycling stability, indicating better structural stability during the charge and discharge. For the synthesis of PBDs, they employed all three steps with ion exchange as the pre-treatment by using NaOH, which simultaneously derived iron hydroxide from the PB template, followed by an annealing step to produce crystalline iron oxide. In another report, Liu *et al.*[67] prepared yolk–shell spheres by coating PB particles with resorcinol formaldehyde. They performed initial annealing and hydrothermal treatment *via* thioacetamide to prepare FeS_2 yolks and carbon shells. The present free space between the yolk and the shell provides room for volumetric expansion, which occurs during the conversion reactions for lithiation and de-lithiation. The shell is not an active material and does not aggregate during the reactions; therefore, a stable cycling performance is achieved.

4.2.3 Hierarchical structure. Hierarchical materials enable macrostructure arrangements with complex morphologies that provide a higher accessible surface area which is critical for applications reliant on surface activity such as catalysis or solar cells. Huang *et al.* prepared nickel sulfide mesospheres made of an assembly of 2D nanoflakes and compared the performance of this material to a similar nickel sulfide phase in nanoparticle

Open Access Article. Published on 15 March 2023. Downloaded on 2/9/2026 11:49:42 AM.
This article is licensed under a Creative Commons Attribution 3.0 Unported Licence.

morphology as a catalyst for solar cells.[94] They started with NiHCCo and performed ion exchange and etching to remove cobalt by using $(NH_4)_2S$ salt and further derivatization *via* a thermal treatment by using sublimed sulfur powder. The hierarchical nanosphere material presented better long-term stability and faster electrolyte regeneration, assigned to lower resistance and diffusion impedance compared to the nanoparticles.

4.2.4 Carbon composite. Using carbonaceous materials with a high ratio of sp^2 hybridized carbon atoms increases the conductivity, whether when used as a carbon coating, a substrate, or a matrix, and is a standard approach in applications that rely on facile electron transfer. Forming a coating has the added benefit of the entrapment of unwanted species. Wu *et al.*[65] explored bimetallic Ni–Co phosphide as a separator and polysulfide mediator in Li–S batteries. To prevent polysulfide shuttling during battery cycling, they designed carbon-coated hollow cages of NiCo phosphide. Although the results are not compared to a coating-less counterpart, successful polysulfide mediation is demonstrated. For this, two strategies are combined: first, a hollow structure to mitigate the volume expansion in polysulfide adsorption, and second, the carbon coating by using polydopamine to entrap these species and increase the capacity stability of the cell. A rather less explored strategy is employing electrospinning to either decorate electrospun fibres by the PBD or to directly electrospin the PBA/D. A 1D structure can be produced by controlling the fibre size and providing a high surface area and active site availability. Moreover, the polymer-based fibre can be heat treated and used as a carbon substrate to increase the overall conductivity of the composite.[70] For example, Wei *et al.*[100] prepared FeCo phosphide on nitrogen-doped carbon fibres through electrospinning. They further annealed and calcined the material and then performed a second derivatization by using NaH_2PO_2 powder as the phosphor source. Electrospinning provides a high surface area and access sites to evenly distributed particles while protecting them from agglomeration due to the open fibre morphology, which aids in the catalytic performance.

5. Summary and outlook

The Prussian blue family of compounds emerged as a new class of precursors/templates for synthesizing advanced materials. They provide a source of different metallic species, carbon, and nitrogen arranged in open framework cubic structures. The cubic morphology can be tuned into various complex, hierarchical, and porous/hollow structures, while composition can be changed through surface modification and ion exchange processes. In addition, the template synthesis is water-based and usually low-cost, making it a sustainable and scalable derivatization template. Such structures can be converted into a wide array of metal-based compound compositions whose morphology is a direct product of the PBA template. Conversion is achieved by different derivatization methodologies, mainly

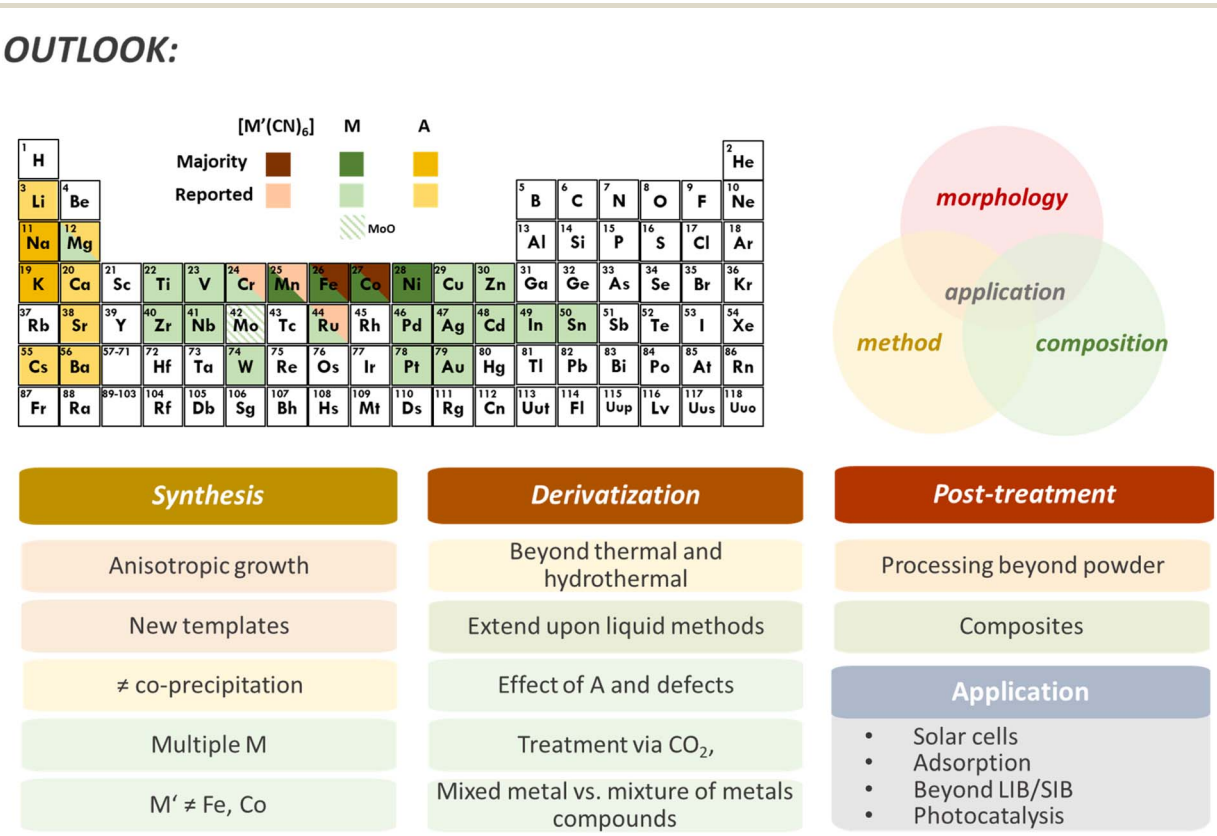

Fig. 5 Outlook on PBDs. Many compositions remain unexplored. Further investigating new synthetic methods, composites and material processing can improve PBD performance in current and new applications.

 This journal is © The Royal Society of Chemistry 2023

Open Access Article. Published on 15 March 2023. Downloaded on 2/9/2026 11:49:42 AM.
This article is licensed under a Creative Commons Attribution 3.0 Unported Licence.

consisting of thermal and hydrothermal methods. Most derivatives are characterized by increased surface area and homogeneous morphology and composition. The different PBDs and their composites have enhanced performance for several applications, such as catalysis and diverse energy storage technologies.

Though PBD reports are quickly growing, several aspects of using PBAs as templates are overlooked. First, regardless of the increased interest in PBDs, most reports are restricted to a limited number of synthetic approaches and compositions. In addition to the classic PBA synthesis route *via* a liquid method, cyanogels can aid in expanding the PBA chemistry past the transition metal combinations.[119,120] The extensive work on PBA synthesis and particle control should be taken advantage of to explore and achieve a well-tailored PBA template for derivatization. In terms of composition, much can be done by temperature control, while the ratio of metals will play a defining role in the phases that can be obtained. Combining multiple M species could also contribute to a more diverse range of compositions. For example, the gradient synthesis of PBAs is an unexplored method for PBDs.[46,47] The gradient enables complex compositions, a mixture of different metal species, and could easily create PBDs with $M_1@M_2$ core–shell structures. Even though PBAs with different M species have been reported, most PBD studies consist of M = Fe, Co, Ni, and Mn (Fig. 5). Meanwhile, a challenge is posed for compositions without Fe and Co, given the availability of $[M'(CN)_6]$ salts. Currently, ion-exchange synthesis seems to be the only described way to remove M′ species, besides specific acid washing for Fe removal.

PBA can show different structures with lower or higher degrees of defects (as in the soluble and insoluble forms) and cation content. However, there is still a lack of understanding of whether and how such defects and cations influence the derivative. For example, a few studies observed the presence of alkali-containing phases in the resulting derivative arising from the PBA alkali-rich structure.[56,63] The counter-cation largely influences PBA structure and properties,[112] therefore, more attention should be given to counter-cations present in the PBA synthesis, as it is retained in derivatization through heat treatment. For example, adding Li^+ in the PBA synthesis could lead to a lithiated PBD phase for energy storage applications. The lack of counter-cations in PBA is associated with a defective structure. Defect engineering is a promising method to introduce inherent conductivity rather than adding other components like carbon, for example, in metal oxides. More insight into the effect of defects in the original PBA structure would help better to design PBA synthesis and pre-treatment for defect-oriented PBDs.

In terms of derivatization methods, liquid methods remain limited, even though they have the advantage of mild/room temperature conditions which can prevent the collapse of highly porous/hollow structures. More elaborate compositions and complex morphologies could arise from diving into liquid ion exchange and etching methods during the pre-treatment and derivatization steps. In this case, post-processing could be limited to low-temperature treatments to induce crystallization, while temperatures for graphitization might be prohibitive. Besides, new experimental approaches could be considered for transforming PBAs into PBDs, like plasma-assisted and electrochemical methods.

When using multiple metallic components, a challenge is to derive single-phase compounds. The weaker bond between M–NC compared to that between M′–CN will likely promote better diffusion of M species upon the heat treatment, which can lead to phase separation.[121] Using a gas with lower reactivity (*e.g.*, CO_2) instead of synthetic air can lower the oxidation rate and retain carbon species. Using H_2S gas instead of sublimed sulfur powder also provides a stable sulfur supply that can result in better homogeneity and control in size and phase.

Much was discussed in terms of morphology change and design during PBD synthesis steps. However, that is mainly done starting from cubic particles. Elaborating on the anisotropic growth of PBA particles could unlock a new range of morphologies and properties of PBDs.[53,54] Expanding on the templating of PBA during their synthesis could also increase the morphological complexity of the resulting PBD. So far, nickel foam is the main adopted substrate for PB growth. Nevertheless, template-oriented growth can be widely varied to produce films, rods, wires, and arrays, among others.[7,122–125]

Most PBA derivatization results in PBD powders for electrochemical applications. This means processing into electrode materials with the aid of binder, carbon, solvents, and coating processes. Exploring new combinations of PBA synthesis and derivatization like electrospinning, aerogels, 3D printed structures, or self-supporting films can enable the preparation of free-standing and flexible PBD materials. Similarly, the PBDs can also be further processed in post-treatment steps to create new composites or assemblies that are not possible before the derivatization method, for example, the addition of conductive polymers (that would otherwise decompose in the treatments), MXenes (that could themselves convert into oxides, sulfides, *etc.*), nanoparticles (that would coarsen), *etc.*

In terms of application, PBAs are primarily used as templates due to the porous structure with ion-compatible voids and high surface area desired in catalysis and energy storage. Nevertheless, each compound class (oxides, sulfides, carbides, *etc.*) has numerous applications. Both selenides and sulfides have essential applications in solar cells, and only a few reports of PBDs address such use.[90,94] Waste treatment is also an overlooked potential application of PBDs. The high porosity and surface area make them ideal for absorption, while the tunable voids and metallic species can induce selectivity towards specific compounds. The HER and OER are primarily studied in the widely explored catalysis field. However, (photo)catalytic degradation could greatly benefit from such structured materials. Iron species are known to provide high photocatalytic efficiency. The straightforward implementation of additional metals like Ti, Sn, or Zn in the PBA synthesis can further tune the catalytic activity. At the same time, target pre-treatment and derivatization can result in a highly active material. Similarly, other energy storage systems besides Li-ion, Li–S, and Na-ion batteries could capitalize on the combination of the

Open Access Article. Published on 15 March 2023. Downloaded on 2/9/2026 11:49:42 AM. This article is licensed under a Creative Commons Attribution 3.0 Unported Licence.

composition and structure of PBDs. For example, the catalytic properties could be used in the ORR in Li–air and Zn–air cathodes.

Using PBA as precursors and templates is an exciting strategy to get unique, specific, and sophisticated materials aiming at target properties and applications. The PBD properties strongly correlate to the PBA structure/composition and the experimental steps employed to derivate the PBA. Exciting scientific and technological challenges emerge from this topic. We expect this review to be useful for chemists, physicists, materials scientists, and engineers interested in exploring this fascinating subject.

Conflicts of interest

There are no conflicts to declare.

Acknowledgements

S. H. acknowledges the funding of the PBDS project (HU 2959/2-1) by the German Research Foundation (DFG, Deutsche Forschungsgemeinschaft). The INM authors thank Eduard Arzt (INM) for his continuing support. A. J. G. Z. thanks INCT Nanocarbono, INCT NanoVida, CAPES, and CNPq for financial support.

References

1 A. A. Karyakin, *Electroanalysis*, 2001, **13**, 813–819.
2 X. Wang and L. Cheng, *Coord. Chem. Rev.*, 2020, **419**, 213393.
3 Q. Wang, J. Li, H. Jin, S. Xin and H. Gao, *InfoMat*, 2022, e12311.
4 H. Yi, R. Qin, S. Ding, Y. Wang, S. Li, Q. Zhao and F. Pan, *Adv. Funct. Mater.*, 2020, **31**, 2006970.
5 S. Zhao, Z. Guo, K. Yan, X. Guo, S. Wan, F. He, B. Sun and G. Wang, *Small Struct.*, 2021, **2**, 2000054.
6 J. Nai and X. W. Lou, *Adv. Mater.*, 2018, **31**, 1706825.
7 B. Kong, C. Selomulya, G. Zheng and D. Zhao, *Chem. Soc. Rev.*, 2015, **44**, 7997–8018.
8 L. Zhang, H. B. Wu and X. W. Lou, *J. Am. Chem. Soc.*, 2013, **135**, 10664–10672.
9 X. Wu, Y. Ru, Y. Bai, G. Zhang, Y. Shi and H. Pang, *Coord. Chem. Rev.*, 2022, **451**, 214260.
10 X. Song, S. Song, D. Wang and H. Zhang, *Small Methods*, 2021, **5**, 2001000.
11 X. Li, L. Yuan, J. Wang, L. Jiang, A. I. Rykov, D. L. Nagy, C. Bogdan, M. A. Ahmed, K. Zhu, G. Sun and W. Yang, *Nanoscale*, 2016, **8**, 2333–2342.
12 C.-H. Chuang, L.-Y. Hsiao, M.-H. Yeh, Y.-C. Wang, S.-C. Chang, L.-D. Tsai and K.-C. Ho, *ACS Appl. Energy Mater.*, 2020, **3**, 11752–11762.
13 Y. Li, J. Hu, K. Yang, B. Cao, Z. Li, L. Yang and F. Pan, *Mater. Today Energy*, 2019, **14**, 100332.
14 B. He, P. Kuang, X. Li, H. Chen, J. Yu and K. Fan, *Chem.–Eur. J.*, 2020, **26**, 4052–4062.
15 X. Wang, A. Dong, Z. Zhu, L. Chai, J. Ding, L. Zhong, T. T. Li, Y. Hu, J. Qian and S. Huang, *Small*, 2020, **16**, 2004614.
16 B. Zhang, J. Shan, J. Yu, W. Wang, W. Li, N. Li and Y. Li, *Int. J. Hydrogen Energy*, 2021, **46**, 8871–8884.
17 D. Liu, R. Qiang, Y. Du, Y. Wang, C. Tian and X. Han, *J. Colloid Interface Sci.*, 2018, **514**, 10–20.
18 Q. Wang, Y. Zhao, W. Luo, W. Jiang, J. Fan, L. Wang, W. Jiang, W.-x. Zhang and J. Yang, *Chem. Commun.*, 2018, **54**, 5887–5890.
19 A. R. Mule, B. Ramulu and J. S. Yu, *Small*, 2022, **18**, 2105185.
20 Y. Lian, H. Sun, X. Wang, P. Qi, Q. Mu, Y. Chen, J. Ye, X. Zhao, Z. Deng and Y. Peng, *Chem. Sci.*, 2019, **10**, 464–474.
21 C. Pei, H. Chen, B. Dong, X. Yu and L. Feng, *J. Power Sources*, 2019, **424**, 131–137.
22 T. Wang, P. Wang, W. Zang, X. Li, D. Chen, Z. Kou, S. Mu and J. Wang, *Adv. Funct. Mater.*, 2022, **32**, 2107382.
23 J. Nai, Y. Lu, L. Yu, X. Wang and X. W. Lou, *Adv. Mater.*, 2017, **29**, 1703870.
24 H. Zhang, Q. Jiang, J. H. Hadden, F. Xie and D. J. Riley, *Adv. Funct. Mater.*, 2021, **31**, 2008989.
25 J. Chen, L. Wei, A. Mahmood, Z. Pei, Z. Zhou, X. Chen and Y. Chen, *Energy Storage Mater.*, 2020, **25**, 585–612.
26 L.-M. Cao, D. Lu, D.-C. Zhong and T.-B. Lu, *Coord. Chem. Rev.*, 2020, **407**, 213156.
27 M. B. Zakaria and T. Chikyow, *Coord. Chem. Rev.*, 2017, **352**, 328–345.
28 A. Azhar, Y. Li, Z. Cai, M. B. Zakaria, M. K. Masud, M. S. A. Hossain, J. Kim, W. Zhang, J. Na, Y. Yamauchi and M. Hu, *Bull. Chem. Soc. Jpn.*, 2019, **92**, 875–904.
29 H. J. Buser, D. Schwarzenbach, W. Petter and A. Ludi, *Inorg. Chem.*, 1977, **16**, 2704–2710.
30 V. D. Neff, *J. Electrochem. Soc.*, 1978, **125**, 886–887.
31 B. Nayebi, K. P. Niavol, B. Nayebi, S. Y. Kim, K. T. Nam, H. W. Jang, R. S. Varma and M. Shokouhimehr, *Mol. Catal.*, 2021, **514**, 111835.
32 Z. Qin, Y. Li and N. Gu, *Adv. Healthcare Mater.*, 2018, **7**, 1800347.
33 W. J. Li, C. Han, G. Cheng, S. L. Chou, H. K. Liu and S. X. Dou, *Small*, 2019, **15**, 1900470.
34 M. Hu, N. L. Torad and Y. Yamauchi, *Eur. J. Inorg. Chem.*, 2012, **2012**, 4795–4799.
35 Z. Shadike, D.-R. Shi, M.-H. Cao, S.-F. Yang, J. Chen and Z.-W. Fu, *J. Mater. Chem. A*, 2017, **5**, 6393–6398.
36 W. Zhang, H. Song, Y. Cheng, C. Liu, C. Wang, M. A. N. Khan, H. Zhang, J. Liu, C. Yu and L. Wang, *Adv. Sci.*, 2019, **6**, 1801901.
37 S. Klink, Y. Ishige and W. Schuhmann, *ChemElectroChem*, 2017, **4**, 490–494.
38 V. Krishnan, A. L. Xidis and V. Neff, *Anal. Chim. Acta*, 1990, **239**, 7–12.
39 K. Itaya, N. Shoji and I. Uchida, *J. Am. Chem. Soc.*, 1984, **106**, 3423–3429.
40 A. Mohammad, P. J. Faustino, M. A. Khan and Y. Yang, *Int. J. Pharm.*, 2014, **477**, 122–127.
41 Q. Hu, X. Huang, Z. Wang, G. Li, Z. Han, H. Yang, X. Ren, Q. Zhang, J. Liu and C. He, *J. Mater. Chem. A*, 2020, **8**, 2140–2146.

 This journal is © The Royal Society of Chemistry 2023

Open Access Article. Published on 15 March 2023. Downloaded on 2/9/2026 11:49:42 AM. This article is licensed under a Creative Commons Attribution 3.0 Unported Licence.

42 L. Xiao, Z. Wang and J. Guan, *Coord. Chem. Rev.*, 2022, **472**, 214777.
43 P. Dvořák, M. Günther, U. Zorn and A. Catsch, *Naunyn-Schmiedebergs Arch. Pharmakol.*, 1971, **269**, 48–56.
44 Z. Chu, Y. Liu and W. Jin, *Biosens. Bioelectron.*, 2017, **96**, 17–25.
45 H. Ming, N. L. Torad, Y.-D. Chiang, K. C.-W. Wu and Y. Yamauchi, *CrystEngComm*, 2012, **14**, 3387–3396.
46 S. Jeon, C. H. Li and D. R. Talham, *Cryst. Growth Des.*, 2021, **21**, 916–925.
47 Y. Li, C. H. Li and D. R. Talham, *Nanoscale*, 2015, **7**, 5209–5216.
48 T.-U. Choi, G. Baek, S. G. Lee and J.-H. Lee, *ACS Appl. Mater. Interfaces*, 2020, **12**, 24817–24826.
49 G. Du and H. Pang, *Energy Storage Mater.*, 2021, **36**, 387–408.
50 L. Catala and T. Mallah, *Coord. Chem. Rev.*, 2017, **346**, 32–61.
51 Z. Li, H. B. Wu and X. W. D. Lou, *Energy Environ. Sci.*, 2016, **9**, 3061–3070.
52 B. Li and H. C. Zeng, *Adv. Mater.*, 2019, **31**, 1801104.
53 F.-X. Bu, M. Hu, W. Zhang, Q. Meng, L. Xu, D.-M. Jiang and J.-S. Jiang, *Chem. Commun.*, 2015, **51**, 17568–17571.
54 M. Cao, X. Wu, X. He and C. Hu, *Chem. Commun.*, 2005, 2241–2243.
55 L. Liu, Z. Hu, L. Sun, G. Gao and X. Liu, *RSC Adv.*, 2015, **5**, 36575–36581.
56 J. Nai, B. Y. Guan, L. Yu and X. W. Lou, *Sci. Adv.*, 2017, **3**, e1700732.
57 J. Nai, J. Zhang and X. W. D. Lou, *Chem*, 2018, **4**, 1967–1982.
58 Y. Wang, J. Ma, J. Wang, S. Chen, H. Wang and J. Zhang, *Adv. Energy Mater.*, 2019, **9**, 1802939.
59 M. Hu, J.-S. Jiang and Y. Zeng, *Chem. Commun.*, 2010, **46**, 1133–1135.
60 M. Hu, S. Furukawa, R. Ohtani, H. Sukegawa, Y. Nemoto, J. Reboul, S. Kitagawa and Y. Yamauchi, *Angew. Chem., Int. Ed.*, 2012, **51**, 984–988.
61 M. Hu, A. A. Belik, M. Imura, K. Mibu, Y. Tsujimoto and Y. Yamauchi, *Chem. Mater.*, 2012, **24**, 2698–2707.
62 Y. Qiu, H. Yang, Y. Cheng, B. Wen and Y. Lin, *Appl. Surf. Sci.*, 2022, **571**, 151334.
63 B. Bornamehr, V. Presser and S. Husmann, *ACS Omega*, 2022, **7**, 38674–38685.
64 M. Jiang, L. Ren, Z. Hou, W. Hua, D. Lei, Y. Cao, Y. Zhang and J.-G. Wang, *J. Power Sources*, 2023, **554**, 232334.
65 Z. Wu, S. Chen, L. Wang, Q. Deng, Z. Zeng, J. Wang and S. Deng, *Energy Storage Mater.*, 2021, **38**, 381–388.
66 N. P. Wickramaratne, V. S. Perera, B.-W. Park, M. Gao, G. W. McGimpsey, S. D. Huang and M. Jaroniec, *Chem. Mater.*, 2013, **25**, 2803–2811.
67 Y. Liu, W. Wang, Q. Chen, C. Xu, D. Cai and H. Zhan, *Inorg. Chem.*, 2019, **58**, 1330–1338.
68 D. Yin, C. Han, X. Bo, J. Liu and L. Guo, *J. Colloid Interface Sci.*, 2019, **533**, 578–587.
69 D. Meng, C. Zhang, Y. Liang, W. Qiu, F. Kong, X. He, M. Chen, P. Liang and Z. Zhang, *J. Colloid Interface Sci.*, 2021, **599**, 280–290.
70 F. Chen, S. Zhang, R. Guo, B. Ma, Y. Xiong, H. Luo, Y. Cheng, X. Wang and R. Gong, *Composites, Part B*, 2021, **224**, 109161.
71 B. Wang, X. Wang, Z. Wang, K. Srinivas, X. Zhang, B. Yu, D. Yang, W. Zhang, T.-C. Lau and Y. Chen, *Chem. Eng. J.*, 2021, **420**, 130481.
72 S.-C. Wang, D. Xiong, C. Chen, M. Gu and F.-Y. Yi, *J. Power Sources*, 2020, **450**, 227712.
73 S. Husmann and A. J. G. Zarbin, *Chem.–Eur. J*, 2016, **22**, 6643–6653.
74 Z. Ding, H. Yu, X. Liu, N. He, X. Chen, H. Li, M. Wang, Y. Yamauchi, X. Xu and M. A. Amin, *J. Colloid Interface Sci.*, 2022, **616**, 210–220.
75 Q. Zong, Y. Zhu, Q. Wang, H. Yang, Q. Zhang, J. Zhan and W. Du, *Chem. Eng. J.*, 2020, **392**, 123664.
76 X. Xu, H. Liang, F. Ming, Z. Qi, Y. Xie and Z. Wang, *ACS Catal.*, 2017, **7**, 6394–6399.
77 Y. Du, J. Chen, L. Li, H. Shi, K. Shao and M. Zhu, *ACS Sustainable Chem. Eng.*, 2019, **7**, 13523–13531.
78 S. Li, L. Bai, H. Shi, X. Hao, L. Chen, Z. Ma, X. Qin and G. Shao, *Int. J. Hydrogen Energy*, 2021, **46**, 27883–27890.
79 F. Ma, Q. Wu, M. Liu, L. Zheng, F. Tong, Z. Wang, P. Wang, Y. Liu, H. Cheng, Y. Dai, Z. Zheng, Y. Fan and B. Huang, *ACS Appl. Mater. Interfaces*, 2021, **13**, 5142–5152.
80 D.-W. Wang, Y.-D. Zhu, S. Lei, S.-M. Chen, Z.-G. Gu and J. Zhang, *J. Solid State Chem.*, 2021, **293**, 121779.
81 K. Wang, F. Zhang, G. Zhu, H. Zhang, Y. Zhao, L. She and J. Yang, *ACS Appl. Mater. Interfaces*, 2019, **11**, 33082–33090.
82 J. Huang, P. Xu, T. Gao, J. Huangfu, X.-j. Wang, S. Liu, Y. Zhang and B. Song, *ACS Sustainable Chem. Eng.*, 2019, **8**, 1319–1328.
83 X. Y. Yu, Y. Feng, Y. Jeon, B. Guan, X. W. Lou and U. Paik, *Adv. Mater.*, 2016, **28**, 9006–9011.
84 X. Liang, G. Wang, W. Gu and G. Ji, *Carbon*, 2021, **177**, 97–106.
85 L. Zhang, H. B. Wu, S. Madhavi, H. H. Hng and X. W. Lou, *J. Am. Chem. Soc.*, 2012, **134**, 17388–17391.
86 L. Hou, L. Lian, L. Zhang, G. Pang, C. Yuan and X. Zhang, *Adv. Funct. Mater.*, 2015, **25**, 238–246.
87 M. Zhang, J. Zhou, J. Yu, L. Shi, M. Ji, H. Liu, D. Li, C. Zhu and J. Xu, *Chem. Eng. J.*, 2019, 123170.
88 G. Tian, X. Ran, Q. Wang and D. Zhang, *Dalton Trans.*, 2022, **51**, 1032–1040.
89 Z. Liu, Y. Wang, R. Chen, C. Chen, H. Yang, J. Ma, Y. Li and S. Wang, *J. Power Sources*, 2018, **403**, 90–96.
90 Q. Zhang, Y. Zhang, T. Zhang, F. Li and L. Xu, *J. Alloys Compd.*, 2023, **930**, 167455.
91 X. Y. Yu, L. Yu, H. B. Wu and X. W. Lou, *Angew. Chem.*, 2015, **54**, 5331–5335.
92 H. Xu, K. Ye, K. Zhu, Y. Gao, J. Yin, J. Yan, G. Wang and D. Cao, *Inorg. Chem. Front.*, 2021, **8**, 2788–2797.
93 Y. Su, D. Ao, H. Liu and Y. Wang, *J. Mater. Chem. A*, 2017, **5**, 8680–8689.
94 S. Huang, H. Wang, Y. Zhang, S. Wang, Z. Chen, Z. Hu and X. Qian, *RSC Adv.*, 2018, **8**, 5992–6000.
95 Y. Song, X. Zhao and Z.-H. Liu, *Electrochim. Acta*, 2021, **374**, 137962.

Open Access Article. Published on 15 March 2023. Downloaded on 2/9/2026 11:49:42 AM.
This article is licensed under a Creative Commons Attribution 3.0 Unported Licence.

96 X. Hu, X. Wang, X. Hu, C. Xie and D. Zeng, *Chem. Commun.*, 2019, **55**, 13386–13389.
97 W. Qi, S. Liu, F. Li, H. Jiang, Z. Cheng, S. Zhao and M. Yang, *Catal. Sci. Technol.*, 2019, **9**, 2571–2577.
98 Z. Cheng, A. Saad, S. Adimi, H. Guo, S. Liu, T. Thomas and M. Yang, *Mater. Adv.*, 2020, **1**, 1161–1167.
99 Z. Wang, S. Jiao, B. Wang, Y. Kang, W. Yin, X. Lv, Q. Zhang, Z. Zhang, Y. Chen and G. Pang, *Int. J. Hydrogen Energy*, 2021, **46**, 8345–8355.
100 B. Wei, G. Xu, J. Hei, L. Zhang and T. Huang, *Int. J. Hydrogen Energy*, 2021, **46**, 2225–2235.
101 X. Ding, W. Uddin, H. Sheng, P. Li, Y. Du and M. Zhu, *J. Alloys Compd.*, 2020, **814**, 152332.
102 X. Zhou, Y. Zi, L. Xu, T. Li, J. Yang and J. Tang, *Inorg. Chem.*, 2021, **60**, 11661–11671.
103 N. Wang, W. Ma, Z. Ren, Y. Du, P. Xu and X. Han, *J. Mater. Chem. A*, 2018, **6**, 884–895.
104 Y.-T. Zhuang, W. Gao, Y.-L. Yu and J.-H. Wang, *Carbon*, 2016, **108**, 190–198.
105 X.-Y. Yu, Y. Feng, B. Guan, X. W. D. Lou and U. Paik, *Energy Environ. Sci.*, 2016, **9**, 1246–1250.
106 M. Du, P. Geng, C. Pei, X. Jiang, Y. Shan, W. Hu, L. Ni and H. Pang, *Angew. Chem.*, 2022, **134**, e202209350.
107 A. Schmidt, S. Husmann and A. J. G. Zarbin, *J. Solid State Electrochem.*, 2018, **22**, 2003–2012.
108 B. Kong, J. Tang, C. Selomulya, W. Li, J. Wei, Y. Fang, Y. Wang, G. Zheng and D. Zhao, *J. Am. Chem. Soc.*, 2014, **136**, 6822–6825.
109 S. Husmann, E. S. Orth and A. J. G. Zarbin, *Electrochim. Acta*, 2019, **312**, 380–391.
110 S. Husmann, A. J. G. Zarbin and R. A. W. Dryfe, *Electrochim. Acta*, 2020, **349**, 136243.
111 X.-J. Zheng, Q. Kuang, T. Xu, Z.-Y. Jiang, S.-H. Zhang, Z.-X. Xie, R.-B. Huang and L.-S. Zheng, *J. Phys. Chem. C*, 2007, **111**, 4499–4502.
112 S. Husmann and A. J. G. Zarbin, *Electrochim. Acta*, 2018, **283**, 1339–1350.
113 C. M. Ferreira, M. K. Ramos and A. J. G. Zarbin, *Eur. J. Inorg. Chem.*, 2021, **2021**, 3373–3384.
114 M. K. Ramos and A. J. G. Zarbin, *Appl. Surf. Sci.*, 2020, **515**, 146000.
115 S. Nakanishi, G. Lu, H. M. Kothari, E. W. Bohannan and J. A. Switzer, *J. Am. Chem. Soc.*, 2003, **125**, 14998–14999.
116 L. C. Lopes, S. Husmann and A. J. G. Zarbin, *Electrochim. Acta*, 2020, **345**, 136199.
117 S. Lei, Q.-H. Li, Y. Kang, Z.-G. Gu and J. Zhang, *Appl. Catal., B*, 2019, **245**, 1–9.
118 R. N. Soek, A. Schmidt, H. Winnischofer and M. Vidotti, *Appl. Surf. Sci.*, 2016, **378**, 253–258.
119 Z. Fang, A. Zhang, P. Wu and G. Yu, *ACS Mater. Lett.*, 2019, **1**, 158–170.
120 P. Wu, A. Zhang, L. Peng, F. Zhao, Y. Tang, Y. Zhou and G. Yu, *ACS Nano*, 2018, **12**, 759–767.
121 P. L. Soni and V. Soni, *The Chemistry of Coordination Complexes and Transition Metals*, CRC Press, 2021.
122 F. Feng, S. Chen, X. Z. Liao and Z. F. Ma, *Small Methods*, 2019, **3**, 1800259.
123 P. Yang, J. Peng, Z. Chu, D. Jiang and W. Jin, *Biosens. Bioelectron.*, 2017, **92**, 709–717.
124 Y. Xian, Y. Hu, F. Liu, Y. Xian, L. Feng and L. Jin, *Biosens. Bioelectron.*, 2007, **22**, 2827–2833.
125 A. Johansson, E. Widenkvist, J. Lu, M. Boman and U. Jansson, *Nano Lett.*, 2005, **5**, 1603–1606.

This journal is © The Royal Society of Chemistry 2023